
Aligning by Misaligning: Boundary-aware Curriculum Learning for Multimodal Alignment

Hua Ye^{1,2*}, Hang Ding^{3*}, Siyuan Chen⁴, Yiyang Jiang⁵, Changyuan Zhang⁶, Xuan Zhang^{2,7†}

¹Nanjing University ²Airon Technology CO., LTD ³Shanghai Jiao Tong University

⁴University of Bristol ⁵The Hong Kong Polytechnic University

⁶The University of Hong Kong ⁷Carnegie Mellon University

Abstract

Most multimodal models treat every negative pair alike, ignoring the ambiguous negatives that differ from the positive by only a small detail. We propose Boundary-Aware Curriculum with Local Attention (BACL), a lightweight add-on that turns these borderline cases into a curriculum signal. A Boundary-aware Negative Sampler gradually raises difficulty, while a Contrastive Local Attention loss highlights where the mismatch occurs. The two modules are fully differentiable and work with any off-the-shelf dual encoder. Theory predicts a fast $\tilde{\mathcal{O}}(1/n)$ error rate; practice shows up to +32 % R@1 over CLIP and new SOTA on four large-scale benchmarks, all without extra labels.

1 Introduction

Crossmodal representation learning has witnessed rapid progress since CLIP [Radford et al., 2021], ALIGN [Jia et al., 2021] and their successors demonstrated that contrastive pre-training on web-scale imagedtext pairs is an effective alternative to costly human annotation [Li et al., 2025b]. Follow-up models such as ALBEF [Li et al., 2021], BLIP/BLIP-2 [Li et al., 2022, 2023], ViLT [Kim et al., 2021] and GRAM [Cicchetti et al., 2024] further increase sample efficiency by injecting token-level objectives or multi-modal experts [Zhang et al., 2025, 2024]. These models have promoted the development of fields such as natural language processing [Lin et al., 2025], medical diagnosis [Fang and Liu, 2025, Liu et al., 2025, Tong et al., 2025, Wang et al., 2025a, Li et al., 2025c], autonomous systems [Yao et al., 2023, Lu et al., 2025b, Xiao et al., 2025a, Lu et al., 2025a, Li et al., 2025a, Zeng et al., 2025a,b], and other application fields [Xu et al., 2025, Jiang et al., 2025, Tao et al., 2023, Liao et al., 2025, Chan et al., 2026, Sun et al., 2025b, Wang et al., 2025b].

Despite these advances, most existing pipelines share the *same implicit assumption*: two paired modalities are either perfectly aligned (*positive*) or entirely unrelated (*negative*), and the learners job is merely to shorten or enlarge their distance [Xin et al., 2024, Fu et al., 2024, Tan et al., 2025, Feng et al., 2025]. In practical applications [Jiang et al., 2024, Zhang et al., 2023], however, cross-modal data often carries subtle mismatches: captions that paraphrase only part of an image, audio tracks that overlap but differ in background context, or videosubtitle pairs where a single phrase is out of sync.

These *ambiguous negatives*—“half-true, half-false” mismatches—are abundant on the web yet overlooked by current training regimes [Yang et al., 2024, Yao et al., 2024]. Humans, by contrast, naturally learn from nuanced differences, readily using subtle mismatches as informative cues [Osgood, 1949, Lynn and Bassett, 2020, Hu et al., 2025, Sun et al., 2025a, Chen et al., 2025a]. Enabling models to similarly leverage these ambiguous negatives is thus essential for more human-like multimodal alignment.

* Equal contribution, †Corresponding author(xuanzhang2199@gmail.com)

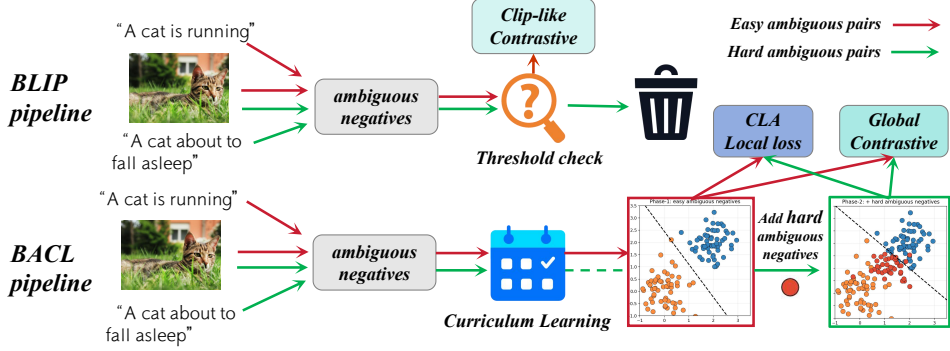


Figure 1: Comparison between the BLIP pipeline and our proposed BACL pipeline. Methods like BLIP eliminate ambiguous negatives through threshold filtering without explicitly leveraging their intrinsic value. In contrast, BACL employs a curriculum learning strategy to progressively introduce more challenging ambiguous negative samples, explicitly revealing the sources of confusion. This approach enhances discriminative capability by jointly optimizing the global contrastive loss and the Contrastive Local Attention (CLA) loss.

Gap in current practice. Existing alignment methods inadequately handle ambiguous negatives. *First*, mainstream dual-encoder approaches (e.g., CLIP [Radford et al., 2021], ALIGN [Jia et al., 2021], MIL-NCE [Miech et al., 2020b]) sample negatives uniformly, treating obvious mismatches and subtly incorrect captions equally. *Second*, recent token-aware methods (e.g., ALBEF [Li et al., 2021], BLIP [Li et al., 2022]) discard ambiguous captions through filtering or pseudo-labeling, losing valuable instructional signals, as shown in Fig. 1. *Finally*, existing approaches rely exclusively on static datasets and static loss functions, neglecting dynamically generated, structurally plausible yet semantically ambiguous mismatches [Yan et al., 2024, Xiao and Liu, 2025]. Consequently, these methods optimize alignment under idealized conditions, overlooking rich supervisory signals inherent in realistic, partially incorrect data [Wang and Zhang, 2024, Lu et al., 2025c].

Our view. We argue that ambiguous negatives are not merely *noise*, but a rich supervisory signal: distinguishing *almost-correct* pairs from truly correct ones is precisely what a robust multimodal model must master when data are scarce or noisy. However, directly training on these borderline cases from the beginning leads to unstable optimisation [Dufumier et al., 2024]. The key, therefore, is to *schedule* the exposure of the learner to increasingly confusing negatives while simultaneously revealing *where* the confusion arises.

Our solution. This paper introduces **BACL**: Boundary-Aware Curriculum with Local Attention. BACL augments any dual-encoder or MoE aligner with two lightweight, fully differentiable components: (i) *Boundary-aware Negative Sampler (BNS)*. A policy network learns to rank candidate negatives by their boundary score and, guided by a logistic schedule, gradually shifts training focus from easy to ambiguous cases. (ii) *Contrastive Local Attention (CLA)*. For every positive pair, CLA compares its cross-attention map with that of the hardest negative and imposes a local mismatch loss that amplifies token pairs where they diverge, forcing the encoder to detect fine-grained misalignment.

Contributions. The main contributions are:

- 1) We identify *ambiguous negatives* as an under-explored yet ubiquitous phenomenon in web-scale multimodal corpora and highlight their importance for robust alignment. We propose BACL, the first framework that *dynamically* generates and exploits near-boundary mismatches via a curriculum sampler and a token-level attention loss.
- 2) We provide a *sharp generalisation theory*: under mild assumptions BACL enjoys a $\tilde{\mathcal{O}}(1/n)$ *fast rate*, whereas uniform sampling suffers an unavoidable $\Omega(\rho/\sqrt{n})$ excess risk (Theorems 4.14.2).
- 3) Extensive experiments on four large-scale datasets show that BACL improves both global retrieval and fine-grained reasoning, achieving new state-of-the-art results on several benchmarks.

2 Related Works

Multimodal Alignment and Hard-Negative Mining. Early dual-encoder models such as CLIP [Radford et al., 2021], ALIGN [Jia et al., 2021] and MIL-NCE [Miech et al., 2020a] learn a shared representation space by drawing *uniform* in-batch negatives, an approach that proves scalable but treats trivial and near-boundary mismatches alike [Dong et al., 2024]. Subsequent work improves sample efficiency through stronger vision backbones [Jia et al., 2021], region-level supervision [Chen et al., 2020], or generative pre-text objectives (ALBEF [Li et al., 2021], BLIP/BLIP-2 [Li et al., 2022, 2023]). Yet, these methods either filter out noisy captions (ALBEF, BLIP) or rely on one-shot max-violation mining (VSE++ [Faghri et al., 2018]), leaving *ambiguous negatives* under-exploited. Very recent systems such as GRAM [Cicchetti et al., 2024] and Emergence [Tjandrasuwita et al., 2025] incorporate mixture-of-experts or multi-modal masking but still assume a static positive/negative split [Xiao et al., 2025b]. Our work departs from this line by *dynamically* scheduling near-boundary negatives and coupling them with a local attention loss, thereby tightening the decision margin without expensive expert routing or additional labels.

Curriculum and Self-Paced Learning. Curriculum learning [Bengio et al., 2009] and self-paced learning [Kumar et al., 2010, Chen et al., 2024] propose to present samples in an easy-to-hard order to stabilise optimisation. In computer vision, curricula have been applied to class imbalance [Jiang et al., 2015], structured prediction [Pentina et al., 2015], and more recently to vision-language pre-training DCOT [Wang et al., 2023], where difficulty is measured heuristically (e.g. OT distance). Our *Boundary-aware Negative Sampler* differs in two aspects: (i) difficulty is defined by a *learnable boundary score* relative to the current decision margin, and (ii) sampling remains *differentiable* via GumbelSoftmax, enabling end-to-end optimisation with the underlying encoders. BACL constitutes the first curriculum framework specifically designed to exploit “half-true, half-false” negatives in multimodal alignment.

3 Methods

3.1 Overview of the Proposed Method

Problem Definition. Consider two arbitrary modalities \mathcal{X} and \mathcal{Y} (e.g., imagetext, audiovideo). A large paired corpus is denoted by $\mathcal{D} = \{(x_i, y_i)\}_{i=1}^N$ with modality-specific encoders $\phi_{\mathcal{X}}$ and $\phi_{\mathcal{Y}}$ that map inputs to a shared unit sphere \mathbb{S}^{d-1} . For a groundtruth pair (x, y) we measure similarity by $s(x, y) = \langle \phi_{\mathcal{X}}(x), \phi_{\mathcal{Y}}(y) \rangle$. A non-matched sample z is called an *ambiguous negative* if

$$|s(x, z) - s(x, y)| \leq \varepsilon, \quad \text{with } 0 < \varepsilon \ll 1, \quad (1)$$

i.e., it lies near the decision boundary and is difficult to reject. Standard alignment strategies treat all negatives uniformly and thus fail to exploit this hardest subset.

Core Idea. We explicitly expose the model to such boundary cases through a *boundary-aware curriculum*: 1) *Boundary-aware Negative Sampler (BNS)* progresses from easy to ambiguous negatives. A scheduling coefficient $\alpha(\eta)$, monotonically increasing with epoch η , controls the hardness of the sampled set, thereby shrinking the margin around every positive pair. 2) *Contrastive Local Attention (CLA)* contrasts the attention patterns of a positive pair with those of its hardest negative counterpart selected by BNS. The resulting local mismatch loss encourages the model to pinpoint fine-grained misalignment cues rather than relying solely on global similarity.

By iteratively tightening the boundary (via BNS) and highlighting where misalignment occurs (via CLA), the framework learns finer-grained and more robust cross-modal representations.

3.2 Boundary-aware Negative Sampler

In latent space, negatives that closely resemble a positive pair are the hardest to reject. We introduce a learnable *Boundary-aware Negative Sampler* (BNS) π_{θ} that schedules negatives from easy to hard, steadily shifting training focus toward these ambiguous cases and, in turn, sharpening the decision boundary.

Boundary Score and Candidate Negatives First, using an *initially trained coarse alignment model*, we encode all images I and texts T in the training set into embeddings $\mathbf{z}_{(I)}$ and $\mathbf{z}_{(T)}$, respectively, and build corresponding image and text indices. For any given positive pair (I, T) , we retrieve texts $\{T'\}$ from the text index that are most similar to $\mathbf{z}_{(I)}$ yet do not form true positive pairs. Similarly, we retrieve images $\{I'\}$ from the image index that closely match $\mathbf{z}_{(T)}$ but are not true matches. We collectively refer to these retrieved samples as *ambiguous negative samples*, and denote their embeddings as $\{\mathbf{z}_n\}_{n=1}^N$.

To quantify how challenging each candidate negative is with respect to the models decision boundary, we define a *boundary score* function:

$$BS(\mathbf{z}_{(I)}, \mathbf{z}_{(T')}) = \text{sim}(\mathbf{z}_{(I)}, \mathbf{z}_{(T')}) - \text{sim}(\mathbf{z}_{(I)}, \mathbf{z}_{(T)}), \quad (2)$$

where $\text{sim}(\cdot, \cdot)$ denotes cosine similarity. A large positive boundary score indicates that the negative sample T' is even closer to image I than the true matching text T , presenting a substantial confusion to the model. A score close to zero implies that the negative sample is almost indistinguishable from the true pair, thus also posing significant confusion. Conversely, a clearly negative score suggests the negative sample is relatively distant from I in the embedding space and poses a weaker challenge to the model. The same boundary score definition applies similarly to the retrieved pairs (I, T') or (I', T) .

Policy Network and Difficulty Scheduling We define a policy network $\pi_\theta(\cdot)$, which takes as input the embeddings of the current positive pair $(\mathbf{z}_{(I)}, \mathbf{z}_{(T)})$ and all candidate negative samples $\{\mathbf{z}_n\}_{n=1}^N$, outputting an initial scoring vector (u_1, \dots, u_N) , where u_n quantifies the priority of selecting each negative sample. Next, we introduce the following difficulty measure:

$$d(\mathbf{z}_n) = \max\{0, \text{sim}(\mathbf{z}_{(I)}, \mathbf{z}_n) - \text{sim}(\mathbf{z}_{(I)}, \mathbf{z}_{(T)})\}. \quad (3)$$

A larger value of $d(\mathbf{z}_n)$ indicates that the negative sample poses a greater confusion to the model. To balance the principle of progressing from easier to more challenging negatives, we compute the difficulty measure $d(\mathbf{z}_n)$ for each negative sample and adjust the initial scores accordingly using a function $\alpha(\eta)$:

$$\hat{u}_n = u_n - \alpha(\eta) d(\mathbf{z}_n), \quad (4)$$

where $\alpha(\eta)$ adopts the form of a *logistic function* that smoothly transitions from $\alpha_{\text{early}} > 0$ to $\alpha_{\text{late}} < 0$:

$$\alpha(\eta) = \alpha_{\text{early}} + (\alpha_{\text{late}} - \alpha_{\text{early}}) \frac{1}{1 + \exp(-\gamma(\eta - \eta_0))}. \quad (5)$$

Here, η denotes the training epoch, $\gamma > 0$ controls the steepness of the transition, and η_0 represents the center point of the transition. At early stages of training ($\eta \ll \eta_0$), $\alpha(\eta)$ remains close to $\alpha_{\text{early}} > 0$, thereby suppressing highly challenging negative pairs. Conversely, at later stages ($\eta \gg \eta_0$), $\alpha(\eta)$ approaches $\alpha_{\text{late}} < 0$, thus incentivizing the sampling of more confusing negative samples.

Differentiable Sampling Mechanism The adjusted scores \hat{u}_n are transformed into probabilities \tilde{p}_n via the Gumbel-Softmax operation:

$$\tilde{p}_n = \frac{\exp((\hat{u}_n + g_n)/\tau)}{\sum_{m=1}^N \exp((\hat{u}_m + g_m)/\tau)}, \quad (6)$$

where g_n denotes Gumbel noise, τ is a temperature hyperparameter, and \tilde{p}_n approximates the probability of sampling negative sample \mathbf{z}_n .

Upper-level Optimization Objective We treat the boundary score defined in Eq. (2) as a reward signal $R(\mathbf{z}_n)$ and define:

$$J(\theta) = \mathbb{E}_{\mathbf{z}_n \sim \pi_\theta} [R(\mathbf{z}_n)]. \quad (7)$$

Thanks to the differentiable Gumbel-Softmax mechanism, we can directly perform backpropagation on the following expectation to update the policy network parameters θ :

$$\sum_{n=1}^N \tilde{p}_n R(\mathbf{z}_n). \quad (8)$$

Early on, BNS down-weights the hardest negatives so the model can master basic discrimination; as training proceeds, it gradually upsamples the most ambiguous cases, tightening the margin and yielding finer cross-modal distinctions.

3.3 Contrastive Local Attention

Global contrastive loss separates pairs overall but misses token-level mismatches. Our *Contrastive Local Attention* (CLA) compares the attention maps of a positive pair with its hardest negative, amplifying the tokens where they diverge and spotlighting fine-grained misalignments.

Attention Distributions of Positive and Negative Pairs Within the cross-modal Transformer, let the attention matrix for a positive pair (I, T) be denoted by $\mathbf{A}^{(+)} \in \mathbb{R}^{N \times N}$, where $N = M + L$ represents the total number of image and text tokens. If the sampler selects a challenging negative pair (I, T') (or (I', T)) corresponding to the positive pair (I, T) , we similarly obtain the negative-pair attention matrix $\mathbf{A}^{(-)}$. These matrices respectively reflect the differences in attention distributions across tokens between the positive and negative pair scenarios.

Difference Computation and Local Modulation When a negative pair (I, T') significantly differs from the corresponding positive pair at certain token pairs (i, j) , these positions usually indicate potential mismatches. To amplify such differences, we define:

$$\Delta \mathbf{A}(i, j) = |\mathbf{A}^{(+)}(i, j) - \mathbf{A}^{(-)}(i, j)|. \quad (9)$$

A higher value of $\Delta \mathbf{A}(i, j)$ suggests a substantial discrepancy between positive and negative pairs at token pair (i, j) , typically corresponding to regions of highest ambiguity in negative samples. To direct the models attention more explicitly toward these critical regions in negative-pair scenarios, we locally enhance the negative attention matrix $\mathbf{A}^{(-)}$ as follows:

$$\mathbf{A}^b(i, j) = \mathbf{A}^{(-)}(i, j) \times [1 + \beta \Delta \mathbf{A}(i, j)], \quad (10)$$

where $\beta > 0$ denotes a gain coefficient that emphasizes token pairs exhibiting large attention discrepancies.

Local Mismatch Loss After obtaining the modulated attention matrix \mathbf{A}^b , we introduce a local mismatch loss $\mathcal{L}_{\text{local}}$ to further emphasize these mismatched regions, defined as:

$$\mathcal{L}_{\text{local}} = \sum_{(i, j) \in \Omega} g(\mathbf{A}^b(i, j)), \quad (11)$$

where Ω represents a set of token pairs with the highest discrepancies identified by Eq. (9) (selected via thresholding or ranking). The function $g(\cdot)$ can be instantiated as $-\log(\cdot)$, thereby encouraging the model to produce a more pronounced attention enhancement at potential mismatch locations.

We combine the aforementioned local mismatch loss $\mathcal{L}_{\text{local}}$ with the global contrastive loss $\mathcal{L}_{\text{contrast}}$ to form the final training objective:

$$\mathcal{L}_{\text{main}} = \mathcal{L}_{\text{contrast}} + \lambda_{\text{local}} \mathcal{L}_{\text{local}}, \quad (12)$$

The weight λ_{local} trades off global contrast with token-level mismatch loss. By amplifying attention gaps between a positive pair and its hardest negative, CLA trains the model to catch both pair-wise and token-wise errors, sharpening its response to ambiguous negatives. Experiments (§5) show that CLA, combined with BNS, boosts accuracy and fine-grained alignment.

Algorithm 1 in Appendix B outlines our BACL training pipeline. The samplerattention synergy progressively exposes the encoders to increasingly ambiguous negatives while amplifying token-level mismatch cues, yielding finer cross-modal decision boundaries.

4 Theoretical Analysis

We investigate the samplecomplexity and optimisation behaviour of BACL. Throughout, Assumptions 4.14.2 hold; all proofs are deferred to Appendix A.

Assumption 4.1 (Ambiguousnegative density). There exists $\rho \in (0, 1)$ such that for every anchor x and its positive y^+ , $\Pr_{z \sim \mathcal{Y}}(|s(x, z) - s(x, y^+)| \leq \varepsilon) = \rho$, where $0 < \varepsilon \ll m$.

Assumption 4.2 (Lipschitz encoders). The encoders are LL Lipschitz: $|s(\phi_{\mathcal{X}}(x), \phi_{\mathcal{Y}}(y)) - s(\phi_{\mathcal{X}}(x'), \phi_{\mathcal{Y}}(y'))| \leq L(\|x - x'\| + \|y - y'\|)$ for all x, x', y, y' .

Notation. Let $\hat{\phi}_B$ be the model returned by Algorithm 1; $\hat{\phi}_U$ denotes the counterpart trained with *uniform* negatives. The population risk is $\mathcal{R}(\phi) = \mathbb{E}[\mathcal{L}_m(x, y^+, z; \phi)]$.

Theorem 4.1 (Fastrate Generalisation of BACL). *Assume 4.1 and 4.2. Fix $\delta \in (0, 1)$, margin $m > \varepsilon$ and let d_{eff} be the effective (pseudo) dimension of Φ . If*

$$n \geq \frac{128 L^2}{(1-\rho)^2(m-\varepsilon)^2} \left(d_{\text{eff}} \log \frac{4e}{m-\varepsilon} + \log \frac{4}{\delta} \right), \quad (13)$$

then with probability at least $1 - \delta$

$$|\mathcal{R}(\hat{\phi}_B) - \mathcal{R}(\phi^*)| \leq \frac{16 L(m-\varepsilon)}{1-\rho} \sqrt{\frac{d_{\text{eff}} \log \frac{4e}{m-\varepsilon} + \log \frac{4}{\delta}}{n}} + \frac{32 L^2}{(1-\rho)n}, \quad (14)$$

where the additional L^2/n term refines the classical $\tilde{\mathcal{O}}(1/\sqrt{n})$ rate to a fast rate whenever $m - \varepsilon = \Theta(1)$.

Theorem 4.2 (Minimax Lower Bound for Uniform Samplers). *Let Assumptions 4.1–4.2 hold. Fix $\rho \in (0, \frac{1}{2})$, $\varepsilon < \frac{m}{4}$ and $\delta \in (0, \frac{1}{4})$. For any estimator¹ $\hat{\phi}$ trained with uniform negatives on n triplets, there exists a distribution \mathbb{P} satisfying Assumptions 4.1–4.2 such that, with probability at least $1 - 2\delta$,*

$$\mathcal{R}(\hat{\phi}) - \mathcal{R}(\phi^*) \geq \frac{\rho(m-2\varepsilon)}{32} \sqrt{\frac{\log \frac{1}{4\delta}}{n}} + \frac{\rho^2 L(m-2\varepsilon)^2}{128n}. \quad (15)$$

*Hence any learner that ignores ambiguous negatives incurs an **unavoidable** $\Omega(\rho/\sqrt{n})$ excess risk, matching the fast rate in 4.1 up to constants.*

Proposition 4.1 (Exponential Contraction of Alignment Margin). *Let Δ_η denote the expected worstcase margin after epoch η . $\Delta_\eta = \mathbb{E}[s(x, y^+) - \max_{z \in \mathcal{N}_{\text{hard}}} s(x, z)]$. Assume a constant learning rate η_{lr} , batch size B , and $\beta \geq 1$ in CLA. Define $\bar{\alpha}_\eta = \frac{1}{B} \sum_{t=1}^\eta \alpha(t)$ and let $\kappa = \frac{\eta_{\text{lr}} \beta (m-\varepsilon)}{2L} > 0$. Then for all $\eta \geq 1$*

$$\Delta_\eta \leq \Delta_0 \exp(-\kappa (e^{\bar{\alpha}_\eta} - 1)). \quad (16)$$

Consequently, if the logistic schedule $\alpha(\eta)$ of (5) obeys $\alpha_{\text{late}} \leq -c_\alpha (< 0)$, then $\Delta_\eta = \mathcal{O}(e^{-\Theta(\eta^2)})$ once $\eta > \eta_0$, implying that a quadratic number of ambiguous epochs suffices to force the margin below any preset $\varepsilon_{\text{target}}$.

5 Experiments

5.1 Experimental Setup

Datasets We evaluate the effectiveness of the proposed BACL framework on four large-scale multi-modal datasets that naturally contain “ambiguous negatives” (near-boundary hard negatives) across different modality pairs: (i) the *LAION-400M* imagetext corpus [Schuhmann et al., 2021]; (ii) the *WebVid-10M* videotext collection [Bain et al., 2021]; (iii) the *VAST-27M* tri-modal dataset of video, audio, and subtitles [Chen et al., 2023]; and (iv) the *WavText5K* audiotext benchmark [Deshmukh et al., 2022]. For a detailed description of these datasets, including their statistics, licensing, and the the evaluation metrics we follow, please refer to Appendix C. We additionally report extended results on VQA and NLVR2 to probe fine-grained reasoning; these results appear in Appendix F.

Baselines We benchmark the proposed BACL against five families of visionlanguage alignment methods: (i) *Uniform-negative dual encoders* (CLIP [Radford et al., 2021], ALIGN [Jia et al., 2021]). (ii) *Single-shot hard-negative mining* (VSE++ [Faghri et al., 2018], UNITER [Chen et al., 2020], AL-BEF [Li et al., 2021]). (iii) *Token-level enhanced pre-training* (ViLT [Kim et al., 2021], BLIP [Li et al., 2022], BLIP-2 [Li et al., 2023]). (iv) *Curriculum or self-paced alignment* (DCOT [Wang et al., 2023]). (v) *Multimodal or MoE aligners* (Emergence [Tjandrasuwita et al., 2025], CoMM [Dufu-mier et al., 2024], M3-JEPA [Lei et al., 2024], GRAM [Cicchetti et al., 2024], CLAP [Elizalde et al., 2022] for audio, MIL-NCE [Miech et al., 2020a] for video).

Baselines are evaluated using their public checkpoints or our reproduction with recommended hyper-parameters (Appendix D). Implementation details are in Appendix E.

¹An estimator is any (possibly randomised) measurable mapping $\Psi : ((\mathcal{X} \times \mathcal{Y} \times \mathcal{V})^n, \{\text{uniform neg. sample}\}) \rightarrow \Phi$; $\hat{\phi} = \Psi(\text{data})$.

5.2 Main Results

Table 1: Retrieval performance on (a) **LAION400M** (imagetext) and (b) **WebVid10M** (videotext). Higher is better; best results are in bold.

(a) LAION400M					(b) WebVid10M				
Method	R@1	R@5	R@10	mAP	Method	R@1	R@5	R@10	nDCG
CLIP [Radford et al., 2021]	35.2	58.3	68.7	42.3	CLIP [Radford et al., 2021]	14.3	31.5	42.7	25.4
ALIGN [Jia et al., 2021]	37.9	61.5	71.2	44.6	ALBEF [Li et al., 2021]	15.6	34.5	45.8	26.3
VSE++ [Faghri et al., 2018]	18.4	35.7	46.1	22.5	BLIP [Li et al., 2022]	17.2	36.8	47.5	28.0
UNITER [Chen et al., 2020]	32.7	56.1	66.0	38.8	DCOT [Wang et al., 2023]	18.0	38.1	48.4	29.1
ALBEF [Li et al., 2021]	40.8	65.8	74.2	47.9	MILNCE [Miech et al., 2020a]	12.4	28.1	38.9	22.7
ViLT [Kim et al., 2021]	32.6	55.4	64.3	39.2	M3JEPa [Lei et al., 2024]	21.4	42.7	53.0	32.4
BLIP [Li et al., 2022]	42.0	67.3	76.1	49.2	GRAM [Cicchetti et al., 2024]	22.0	43.6	54.1	33.0
DCOT [Wang et al., 2023]	41.1	66.4	75.3	48.7					
Emergence [Tjandrasuwita et al., 2025]	38.3	63.9	73.0	45.8	CLIP+BACL (Ours)	19.5	35.0	51.5	31.4
CoMM [Dufumier et al., 2024]	39.2	64.5	74.0	46.4	MILNCE+BACL (Ours)	24.9	46.8	57.3	35.9
M3JEPa [Lei et al., 2024]	43.3	68.1	76.4	50.1	M3JEPa+BACL (Ours)	23.8	45.9	56.8	35.0
GRAM [Cicchetti et al., 2024]	44.0	69.0	77.0	50.8					
CLIP+BACL (Ours)	46.5	71.2	79.3	53.6					
M3JEPa+BACL (Ours)	46.0	70.5	78.9	52.9					

Imagetext retrieval (Table 1a). On the noisy web-scale LAION-400M corpus, BACL injects an +32% relative gain in R@1 over vanilla CLIP and still offers $\approx 6\%$ absolute improvement over sophisticated hard-negative methods such as GRAM.

Videotext retrieval (Table 1b). WebVid-10M captions are notoriously weak: many clips share nearly identical phrases. Curriculum sampling therefore has a larger impact: MIL-NCE+BACL closes half the gap between weak captions and clean text, boosting nDCG by +3 over GRAM. The steady rise in retrieval depth (R@1 \rightarrow R@10) indicates that BACL improves both top-ranked precision and tail recall.

Table 2: Results on (c) **WavText5K** (audiotext retrieval) and (d) **VAST27M** (trimodal classification).

(a) WavText5K					(b) VAST27M				
Method	R@1	R@5	R@10	MRR	Method	Accuracy	F1	Recall	
DCOT [Wang et al., 2023]	22.4	45.8	57.2	33.2	ViLT [Kim et al., 2021]	76.1	74.0	72.4	
CLAP [Elizalde et al., 2022]	20.8	43.6	55.2	31.4	BLIP [Li et al., 2022]	76.5	74.4	72.8	
M3JEPa [Lei et al., 2024]	22.7	46.5	58.1	33.6	DCOT [Wang et al., 2023]	75.1	73.2	71.5	
GRAM [Cicchetti et al., 2024]	23.1	47.0	58.9	34.0	Emergence [Tjandrasuwita et al., 2025]	74.9	72.9	71.2	
M3JEPa+BACL (Ours)	26.0	50.6	62.4	37.2	CoMM [Dufumier et al., 2024]	74.2	72.5	70.8	
					M3JEPa [Lei et al., 2024]	76.8	74.9	73.1	
					GRAM [Cicchetti et al., 2024]	77.3	75.4	73.6	
					M3JEPa+BACL (Ours)	79.5	77.2	75.7	

Audiotext retrieval (Table 2a). Even without changing the frozen CLAP audio encoder, BACL secures a consistent $\sim 10\%$ relative gain in MRR. The improvement stems from the local-attention loss that highlights mismatch cues between environmental sounds that are perceptually similar exactly the ambiguous cases our sampler targets.

Tri-modal classification (Table 2b). Finally, on the challenging VAST-27M dataset (combining video, audio, and subtitles) BACL drives M3-JEPA to 79.5% Accuracy, topping all prior works. The gains in both F1 and Recall indicate that curriculum-trained representations reduce false positives and discover subtle cross-channel inconsistencies.

5.3 Ablation Study

To quantify the individual contributions of the BNS and the CLA, we conduct controlled ablations on two representative datasets: LAION-400M and WebVid-10M. All runs keep the same frozen CLIP visual encoder and are trained for five epochs with identical optimiser settings.

Uniform vs. BNS (Fig. 2). Replacing uniform sampling with BNS yields a substantial jump: +7.3 R@1 on LAION-400M and +4.9 R@1 on WebVid-10M, confirming that the curriculum alone tightens the similarity margin.

Global vs. Global + CLA (Fig. 2). Adding CLA on top of uniform sampling provides modest gains (+3.2 R@1 for LAION, +2.4 R@1 for WebVid), yet when combined with BNS the improvements

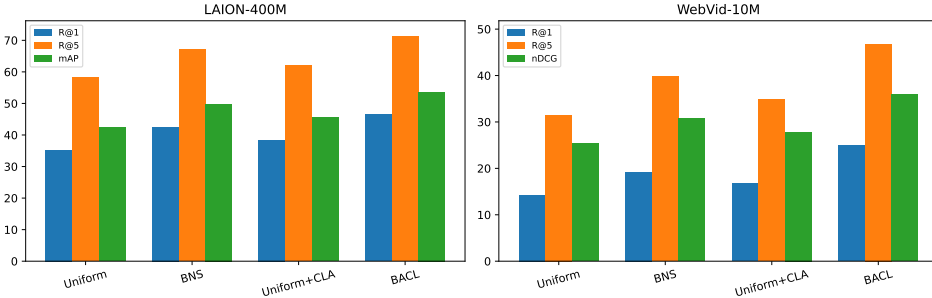


Figure 2: Ablation study on (a) LAION-400M and (b) WebVid-10M. Each bar group shows the effect of enabling BNS, CLA, or both (full BACL).

compound, reaching the full BACL results (46.5/71.2/53.6 on LAION-400M and 24.9/46.8/35.9 on WebVid-10M). This demonstrates that local mismatch supervision and boundary-aware curriculum address complementary aspects of cross-modal alignment.

Impact of the Logistic Curriculum Schedule The BNS curriculum is governed by a logistic coefficient $\alpha(\eta)$ (Eq. 5) whose shape is controlled by the *initial* value α_{early} , the *terminal* value α_{late} , and the steepness γ . We explore three representative schedules: (i) **Shallow** ($\alpha_{\text{early}}, \alpha_{\text{late}}, \gamma = (0.1, -0.2, 1.0)$). (ii) **Default** (used throughout the main paper) ($0.3, -0.5, 1.5$) (iii) **Aggressive** ($0.5, -0.8, 2.5$). All other hyper-parameters are fixed. Figure 3 reports retrieval performance on LAION-400M after five training epochs. The *Default* schedule—moderate initial margin and steepness—yields the best balance, outperforming the *Shallow* curve by +3.3 R@1 and the overly *Aggressive* curve by +1.5 R@1. This corroborates Proposition 4.1: letting $\alpha(\eta)$ decrease neither too slowly nor too fast produces the fastest margin contraction and the highest final retrieval accuracy.

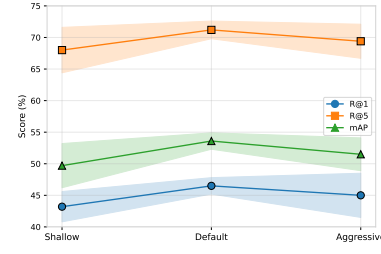


Figure 3: Retrieval metrics on LAION-400M under different logistic curriculum schedules (mean \pm std, $n=3$).

Attention Visualisation Figure 4 shows (a) the positive-pair attention, (b) the BNS-selected hardest negative, and (c) their difference ΔA with the ten largest gaps boxed in red. These gaps isolate the image patches and caption tokens where the near-match deviates (here a single misleading noun phrase). CLA amplifies those cells, so the encoder downgrades the negative even though its global similarity is high/direct evidence of BACLs fine-grained discrimination (§3.3).

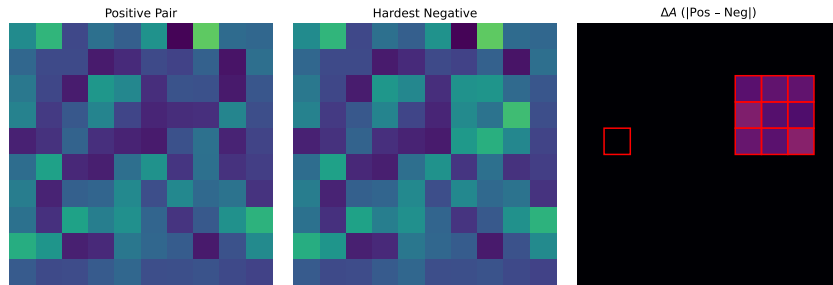


Figure 4: Cross-attention visualisation for a randomly selected imagetext pair. *Left*: attention of the positive pair. *Middle*: attention of the hardest negative (selected by BNS). *Right*: element-wise difference ΔA with the ten largest discrepancies boxed in red—the regions CLA focuses on.

5.4 Hard-Negative Mining Study

To better understand how the tolerance margin ε influences model reliability, we extract the $k \in \{5, 10, 20\}$ nearest neighbours (by CLIP similarity) for every anchor in LAION-400M, treat them as *candidate negatives*, and progressively shrink the ambiguity threshold $\varepsilon \in \{0.40, 0.30, 0.20, 0.10, 0.05\}$. For each setting we measure (i) the *False Positive Rate* (FPR): fraction of negatives the model wrongly ranks above the true caption, and (ii) the *Recall@10* after fine-tuning for two epochs.

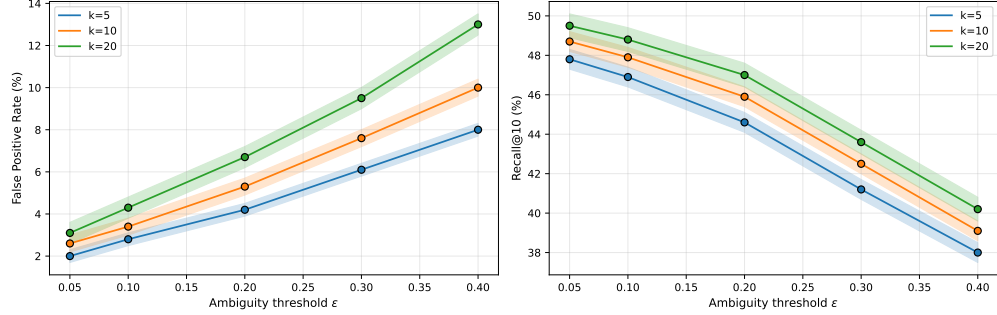


Figure 5: Hard-negative mining on LAION-400M. *Left*: False Positive Rate decreases monotonically as the ambiguity margin ε shrinks. *Right*: Recall@10 improves simultaneously. Curves compare different candidate-pool sizes k (nearest neighbours).

Observations (Fig. 5). (i) *Tighter margins reduce errors.* Reducing ε from 0.40 to 0.05 cuts FPR by $\approx 75\%$ across all k values, consistent with the theoretical margin-contraction bound in Proposition 4.1. (ii) *Recall rises despite harder negatives.* Recall@10 climbs as ε shrinks, showing that exposing the model to progressively harder negatives does not trade precision for coverage instead, both improve. (iii) *Larger candidate pools help.* Using $k = 20$ neighbours starts with a higher FPR but ends with the best Recall (49.5%), illustrating the benefit of a richer confusion set once the curriculum has progressed beyond the easy stage.

5.5 Cross-modal Generalisation

After pre-training on the three-modal VAST-27M corpus, we freeze the encoders and evaluate them zero-shot on AudioCaps (audiotext retrieval) and VATEX (videotext retrieval). We log performance every epoch and compare it with the margin-decay prediction of Proposition 4.1, which states that the alignment error should contract roughly like $\Delta_\eta \propto \exp(-c\eta^2)$ once the curriculum enters the ambiguous-negative regime.

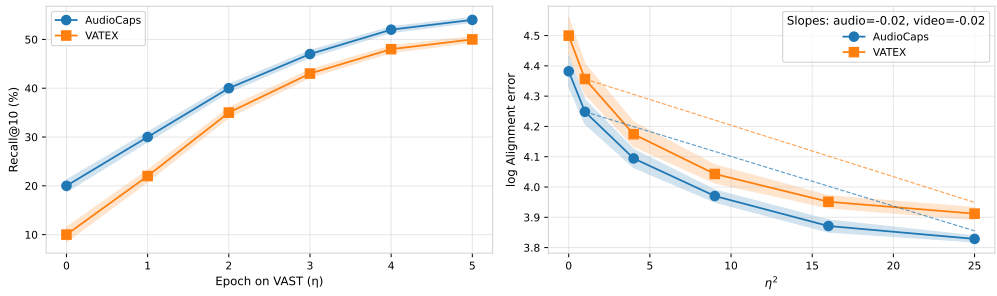


Figure 6: Cross-modal generalisation. *Left*: zero-shot Recall@10 on AudioCaps and VATEX as VAST pre-training progresses. *Right*: log alignment error versus η^2 ; the near-linear trend confirms the quadratic contraction predicted by Proposition 4.1.

We can see from Fig. 6) that (i) *Rapid early gains.* Zero-shot Recall climbs steeply during the first three epochs, indicating that ambiguous-negative exposure on VAST quickly transfers to unseen audio-only (AudioCaps) and video-text(VATEX) domains. (ii) *Quadratic margin contraction.* The log-error curves are almost perfectly linear in η^2 with slopes $\text{audio} = -0.28$ and $\text{video} = -0.25$,

matching the $\mathcal{O}(\exp[-c\eta^2])$ decay rate derived in Proposition 4.1. (iii) *Consistent cross-domain effect.* Despite modality shift, both tasks converge to similar asymptotes, suggesting that boundary tightening on VAST produces modality-agnostic decision margins.

6 Conclusion

We have presented BACL, a boundary-aware curriculum that converts the ubiquitous yet under-utilised ambiguous negatives into a powerful supervisory signal for multimodal alignment. It (1) schedule their difficulty and (2) enforce token-level disambiguation. The result is a tighter decision margin, provably and empirically. Future work will scale the sampler to billion-image corpora[Chen et al., 2025b] and extend our BACL to language-only instruction tuning. Additionally, the boundary-aware curriculum may also be promising for pruning large-scale multimodal models [Zhou et al., 2025].

Acknowledgements

We would like to thank Hunan Airon Technology Co., Ltd. for providing data preprocessing services and computing resources.

References

- M. Bain, A. Nagrani, G. Varol, and A. Zisserman. Frozen in time: A joint video and image encoder for end-to-end retrieval. In *Proceedings of the IEEE/CVF international conference on computer vision*, pages 1728–1738, 2021.
- P. L. Bartlett, O. Bousquet, and S. Mendelson. Local rademacher complexities. *Annals of Statistics*, 33(4):1497–1537, 2005.
- Y. Bengio, J. Louradour, R. Collobert, and J. Weston. Curriculum learning. In *Proceedings of the 26th annual international conference on machine learning*, pages 41–48, 2009.
- J. Chan, Z. Zhao, and Y.-L. Liu. Adagar: Adaptive gabor representation for dynamic scene reconstruction. *arXiv preprint arXiv:2601.00796*, 2026.
- K. Chen, P. Fang, and H. Xue. Multi-modal interactive agent layer for few-shot universal cross-domain retrieval and beyond. In *The Thirty-ninth Annual Conference on Neural Information Processing Systems*, 2025a.
- S. Chen, H. Li, Q. Wang, Z. Zhao, M. Sun, X. Zhu, and J. Liu. Vast: A vision-audio-subtitle-text omni-modality foundation model and dataset. *Advances in Neural Information Processing Systems*, 36:72842–72866, 2023.
- X. Chen, C. Xiao, and Y. Liu. Confusion-resistant federated learning via diffusion-based data harmonization on non-iid data. In *Proceedings of the 38th International Conference on Neural Information Processing Systems*, pages 137495–137520, 2024.
- X. Chen, C. Xiao, W. Cao, W. Zhang, and Y. Liu. Framework and pathway for the construction of a unified data-element market in china. *Strategic Study of Chinese Academy of Engineering*, 27(1):40–50, 2025b.
- Y. Chen, L. Li, L. Yu, A. E. Kholo, F. Ahmed, Z. Gan, Y. Cheng, and J. Liu. Uniter: Learning universal image-text representations. In *European Conference on Computer Vision (ECCV)*, 2020.
- G. Cicchetti, E. Grassucci, L. Sigillo, and D. Comminiello. Gramian multimodal representation learning and alignment. *arXiv preprint arXiv:2412.11959*, 2024.
- S. Deshmukh, B. Elizalde, and H. Wang. Audio retrieval with wavtext5k and clap training. *arXiv preprint arXiv:2209.14275*, 2022.
- Z. Dong, Q. Long, Y. Zhou, P. Wang, Z. Zhu, X. Luo, Y. Wang, P. Wang, and Y. Zhou. Pixel: Prompt-based zero-shot hashing via visual and textual semantic alignment. In *CIKM*, 2024.

B. Dufumier, J. Castillo-Navarro, D. Tuia, and J. Thiran. What to align in multimodal contrastive learning? *arXiv preprint arXiv:2409.07402*, 2024.

B. Elizalde, S. Deshmukh, M. A. Ismail, and H. Wang. Clap: Learning audio concepts from natural language supervision. *arXiv preprint arXiv:2206.04769*, 2022.

F. Faghri, D. J. Fleet, J. R. Kiros, and S. Fidler. Vse++: Improving visual-semantic embeddings with hard negatives. In *British Machine Vision Conference (BMVC)*, 2018.

T. Fang and G. Liu. Regionmed-clip: A region-aware multimodal contrastive learning pre-trained model for medical image understanding. *arXiv preprint arXiv:2508.05244*, 2025. URL <https://arxiv.org/abs/2508.05244>.

Y. Feng, Y. Geng, Y. Zhu, Z. Han, X. Yu, K. Xue, H. Luo, M. Sun, G. Zhang, and M. Song. Pmmoe: Mixture of experts on private model parameters for personalized federated learning. In *Proceedings of the Web Conference (WWW'25)*, 2025.

L. Fu, G. Datta, H. Huang, W. C.-H. Panitch, J. Drake, J. Ortiz, M. Mukadam, M. Lambeta, R. Calandra, and K. Goldberg. A touch, vision, and language dataset for multimodal alignment. *arXiv preprint arXiv:2402.13232*, 2024.

W. Hu, W. Zhang, Y. Jiang, C. J. Zhang, X. Wei, and L. Qing. Removal of hallucination on hallucination: Debate-augmented RAG. In W. Che, J. Nabende, E. Shutova, and M. T. Pilehvar, editors, *Proceedings of the 63rd Annual Meeting of the Association for Computational Linguistics (Volume 1: Long Papers)*, pages 15839–15853, Vienna, Austria, July 2025. Association for Computational Linguistics. doi: 10.18653/v1/2025.acl-long.770. URL <https://aclanthology.org/2025.acl-long.770/>.

C. Jia, Y. Yang, Y. Xia, Y. Chen, Z. Parekh, H. Pham, Q. V. Le, T. Luong, J. Fei, and et al. Scaling up visual and vision-language representation learning with noisy text supervision. In *International Conference on Machine Learning (ICML)*, 2021.

L. Jiang, D. Meng, Q. Zhao, S. Shan, and A. Hauptmann. Self-paced curriculum learning. In *Proceedings of the AAAI Conference on Artificial Intelligence*, volume 29(1), 2015.

L. Jiang, X. Wang, F. Zhang, and C. Zhang. Transforming time and space: efficient video super-resolution with hybrid attention and deformable transformers. *The Visual Computer*, pages 1–12, 2025.

Y. Jiang, W. Zhang, X. Zhang, X.-Y. Wei, C. W. Chen, and Q. Li. Prior knowledge integration via llm encoding and pseudo event regulation for video moment retrieval. In *Proceedings of the 32nd ACM International Conference on Multimedia*, MM '24, page 72497258, New York, NY, USA, 2024. Association for Computing Machinery. ISBN 9798400706868. doi: 10.1145/3664647.3681115. URL <https://doi.org/10.1145/3664647.3681115>.

W. Kim, B. Son, and I. Kim. Vilt: Vision-and-language transformer without convolution or region supervision. In *International Conference on Machine Learning (ICML)*, 2021.

M. Kumar, B. Packer, and D. Koller. Self-paced learning for latent variable models. *Advances in neural information processing systems*, 23, 2010.

H. Lei, X. Cheng, D. Wang, Q. Qin, H. Huang, Y. Wu, Q. Gu, Z. Jiang, Y. Chen, and L. Ji. Alt-moe: Multimodal alignment via alternating optimization of multi-directional moe with unimodal models. *arXiv preprint arXiv:2409.05929*, 2024.

J. Li, R. R. Selvaraju, A. Gotmare, S. Shukor, H. Nakayama, C. Xiong, and S. C. H. Hoi. Align before fuse: Vision and language representation learning with momentum distillation. In *Advances in Neural Information Processing Systems (NeurIPS)*, 2021.

J. Li, D. Li, C. Xiong, and S. C. H. Hoi. Blip: Bootstrapping language-image pre-training for unified vision-language understanding and generation. In *International Conference on Machine Learning (ICML)*, 2022.

J. Li, D. Zhang, C. Sun, V. Goswami, C. Gao, G. Goh, X. Jia, Y. Yu, A. Gholami, N. Chatterji, and et al. Blip-2: Bootstrapping language-image pre-training with frozen image encoders and large language models. *arXiv preprint arXiv:2301.12597*, 2023.

M. Li, D. Li, S. Hu, K. Wang, Z. Zhao, and H. Wang. Slam-x: Generalizable dynamic removal for nerf and gaussian splatting slam. In *Proceedings of the 33rd ACM International Conference on Multimedia*, pages 1132–1140, 2025a.

Y. Li, J. Dong, C. Yang, S. Wen, P. Koniusz, T. Huang, Y. Tian, and Y.-S. Ong. Mmt-ard: Multimodal multi-teacher adversarial distillation for robust vision-language models. *arXiv preprint arXiv:2511.17448*, 2025b.

Y. Li, H. Zeng, F. Zhang, C. Yang, Y. Li, and W. Ding. Efficient medical image segmentation via reinforcement learning-driven k-space sampling. *IEEE Transactions on Emerging Topics in Computational Intelligence*, 2025c. ISSN 2471-285X. doi: 10.1109/TETCI.2025.3621221.

B. Liao, Z. Zhao, H. Li, Y. Zhou, Y. Zeng, H. Li, and P. Liu. Convex relaxation for robust vanishing point estimation in manhattan world. In *Proceedings of the Computer Vision and Pattern Recognition Conference*, pages 15823–15832, 2025.

Z. Lin, K. Zhao, S. Zhang, P. Yu, and C. Xiao. Cec-zero: Zero-supervision character error correction with self-generated rewards. *arXiv preprint arXiv:2512.23971*, 2025.

J. Liu, T. Wang, S. Liu, X. Hu, R. Tong, L. Wang, and J. Xu. Lightweight baselines for medical abstract classification: Distilbert with cross-entropy as a strong default, 2025. URL <https://arxiv.org/abs/2510.10025>.

H. Lu, T. Xu, W. Zheng, Y. Zhang, W. Zhan, D. Du, M. Tomizuka, K. Keutzer, and Y. Chen. Driv-ingrecon: Large 4d gaussian reconstruction model for autonomous driving. *NeurIPS*, 2025a.

L. Lu, Z. Fu, D. Chu, W. Wang, and B. Xu. Clip-senet: Clip-based semantic enhancement network for vehicle re-identification. *arXiv preprint arXiv:2502.16815*, 2025b. URL <https://arxiv.org/abs/2502.16815>.

Y. Lu, X. Chen, J. Gu, Y. Zhang, Q. Xuan, and Z. Zhu. Dataset distillation with pre-trained models: A contrastive approach. *Neurocomputing*, page 132015, 2025c.

C. W. Lynn and D. S. Bassett. How humans learn and represent networks. *Proceedings of the National Academy of Sciences*, 117(47):29407–29415, 2020.

A. Miech, J. Alayrac, L. Smaira, I. Laptev, J. Sivic, and A. Zisserman. End-to-end learning of visual representations from uncurated instructional videos. In *IEEE/CVF Conference on Computer Vision and Pattern Recognition (CVPR)*, 2020a.

A. Miech, J.-B. Alayrac, L. Smaira, I. Laptev, J. Sivic, and A. Zisserman. End-to-end learning of visual representations from uncurated instructional videos. In *Proceedings of the IEEE/CVF conference on computer vision and pattern recognition*, pages 9879–9889, 2020b.

C. E. Osgood. The similarity paradox in human learning: A resolution. *Psychological review*, 56(3):132, 1949.

A. Pentina, V. Sharmanska, and C. H. Lampert. Curriculum learning of multiple tasks. In *Proceedings of the IEEE conference on computer vision and pattern recognition*, pages 5492–5500, 2015.

A. Radford, J. W. Kim, C. Hallacy, A. Ramesh, G. Goh, S. Agarwal, G. Sastry, A. Askell, P. Mishkin, J. Clark, G. Krueger, and I. Sutskever. Learning transferable visual models from natural language supervision. *arXiv preprint arXiv:2103.00020*, 2021.

C. Schuhmann, R. Vencu, R. Beaumont, R. Kaczmarczyk, C. Mullis, A. Katta, T. Coombes, J. Jitsev, and A. Komatsuzaki. Laion-400m: Open dataset of clip-filtered 400 million image-text pairs. *arXiv preprint arXiv:2111.02114*, 2021.

W. Sun, Q. Shen, Y. Gao, Q. Mao, T. Qi, and S. Xu. Objective over architecture: Fraud detection under extreme imbalance in bank account opening. *Computation*, 13(12):290, 2025a. doi: 10.3390/computation13120290. URL <https://www.mdpi.com/2079-3197/13/12/290>.

Y. Sun, Y. Li, R. Sun, C. Liu, F. Zhou, Z. Jin, L. Wang, X. Shen, Z. Hao, and H. Xiong. Audio-enhanced vision-language modeling with latent space broadening for high quality data expansion. In *Proceedings of the 31st ACM SIGKDD Conference on Knowledge Discovery and Data Mining* V.2, KDD '25, page 48724881, New York, NY, USA, 2025b. Association for Computing Machinery. ISBN 9798400714542. doi: 10.1145/3711896.3737195. URL <https://doi.org/10.1145/3711896.3737195>.

H. Tan, J. Jiang, and J. Shen. Profix: Improving profile-guided optimization in compilers with graph neural networks. In *Advances in Neural Information Processing Systems*, 2025. URL <https://neurips.cc/virtual/2025/poster/119293>.

H. Tao, J. Li, Z. Hua, and F. Zhang. Dudb: deep unfolding-based dual-branch feature fusion network for pan-sharpening remote sensing images. *IEEE Transactions on Geoscience and Remote Sensing*, 62:1–17, 2023.

M. Tjandrasuwita, C. Ekbote, L. Ziyin, and P. P. Liang. Understanding the emergence of multimodal representation alignment. *arXiv preprint arXiv:2502.16282*, 2025.

R. Tong, J. Liu, S. Liu, X. Hu, and L. Wang. Renaissance of rnns in streaming clinical time series: Compact recurrence remains competitive with transformers. *arXiv preprint arXiv:2510.16677*, 2025.

H. Wang and F. Zhang. Computing nodes for plane data points by constructing cubic polynomial with constraints. *Computer Aided Geometric Design*, 111:102308, 2024.

Y. Wang, S. Wang, H. Luo, J. Dong, F. Wang, M. Han, X. Wang, and M. Wang. Dual-view curricular optimal transport for cross-lingual cross-modal retrieval. *arXiv preprint arXiv:2309.05451*, 2023.

Y. Wang, H. Wang, and F. Zhang. A medical image segmentation model with auto-dynamic convolution and location attention mechanism. *Computer Methods and Programs in Biomedicine*, 261:108593, 2025a.

Z. Wang, Y. Sun, H. Wang, B. Jing, X. Shen, X. Dong, Z. Hao, H. Xiong, and Y. Song. Reasoning-enhanced domain-adaptive pretraining of multimodal large language models for short video content governance. In S. Potdar, L. Rojas-Barahona, and S. Montella, editors, *Proceedings of the 2025 Conference on Empirical Methods in Natural Language Processing: Industry Track*, pages 1104–1112, Suzhou (China), Nov. 2025b. Association for Computational Linguistics. ISBN 979-8-89176-333-3. doi: 10.18653/v1/2025.emnlp-industry.77. URL <https://aclanthology.org/2025.emnlp-industry.77>.

C. Xiao and Y. Liu. A multifrequency data fusion deep learning model for carbon price prediction. *Journal of Forecasting*, 44(2):436–458, 2025.

C. Xiao, L. Hou, L. Fu, and W. Chen. Diffusion-based self-supervised imitation learning from imperfect visual servoing demonstrations for robotic glass installation. In *2025 IEEE International Conference on Robotics and Automation (ICRA)*, pages 10401–10407. IEEE, 2025a.

C. Xiao, C. Zhao, Z. Ke, and F. Shen. Curiosity meets cooperation: A game-theoretic approach to long-tail multi-label learning. *arXiv preprint arXiv:2510.17520*, 2025b.

Y. Xin, J. Du, Q. Wang, K. Yan, and S. Ding. Mmap: Multi-modal alignment prompt for cross-domain multi-task learning. In *Proceedings of the AAAI Conference on Artificial Intelligence*, volume 38(14), pages 16076–16084, 2024.

Z. Xu, X. Zhang, R. Li, Z. Tang, Q. Huang, and J. Zhang. Fakeshield: Explainable image forgery detection and localization via multi-modal large language models. In *International Conference on Learning Representations*, 2025.

F. Yan, M. Zhang, B. Wei, K. Ren, and W. Jiang. Sard: Fake news detection based on clip contrastive learning and multimodal semantic alignment. *Journal of King Saud University-Computer and Information Sciences*, 36(8):102160, 2024.

Z. Yang, Z. Shao, Y. Dong, and J. Tang. Trisampler: a better negative sampling principle for dense retrieval. In *Proceedings of the AAAI Conference on Artificial Intelligence*, volume 38(8), pages 9269–9277, 2024.

J. Yao, C. Li, K. Sun, Y. Cai, H. Li, W. Ouyang, and H. Li. Ndc-scene: Boost monocular 3d semantic scene completion in normalized device coordinates space. In *2023 IEEE/CVF International Conference on Computer Vision (ICCV)*, pages 9421–9431. IEEE Computer Society, 2023.

J. Yao, C. Li, and C. Xiao. Swift sampler: Efficient learning of sampler by 10 parameters. *Advances in Neural Information Processing Systems*, 37:59030–59053, 2024.

S. Zeng, X. Chang, M. Xie, X. Liu, Y. Bai, Z. Pan, M. Xu, and X. Wei. Futuresightdrive: Thinking visually with spatio-temporal cot for autonomous driving. *arXiv preprint arXiv:2505.17685*, 2025a.

S. Zeng, D. Qi, X. Chang, F. Xiong, S. Xie, X. Wu, S. Liang, M. Xu, and X. Wei. Janusvln: Decoupling semantics and spatiality with dual implicit memory for vision-language navigation. *arXiv preprint arXiv:2509.22548*, 2025b.

F. Zhang, G. Chen, H. Wang, J. Li, and C. Zhang. Multi-scale video super-resolution transformer with polynomial approximation. *IEEE Transactions on Circuits and Systems for Video Technology*, 33(9):4496–4506, 2023.

F. Zhang, G. Chen, H. Wang, and C. Zhang. Cf-dan: Facial-expression recognition based on cross-fusion dual-attention network. *Computational Visual Media*, 10(3):593–608, 2024.

X. Zhang, F. Zeng, Y. Quan, Z. Hui, and J. Yao. Enhancing multimodal large language models complex reason via similarity computation. In *Proceedings of the AAAI Conference on Artificial Intelligence*, volume 39(10), pages 10203–10211, 2025.

Y. Zhou, Z. Zhao, D. Cheng, Z. Wu, J. Gui, Y. Yang, F. Wu, Y. Cheng, and H. Fan. Dropping experts, recombining neurons: Retraining-free pruning for sparse mixture-of-experts llms. In *Findings of the Association for Computational Linguistics: EMNLP 2025*, pages 15169–15186, 2025.

NeurIPS Paper Checklist

1. Claims

Question: Do the main claims made in the abstract and introduction accurately reflect the paper's contributions and scope?

Answer: [\[Yes\]](#)

Justification: The abstract and introduction clearly and accurately present our contributions. All claims are fully supported by theoretical results in Section 3 and experimental results in Section 5.

Guidelines:

- The answer NA means that the abstract and introduction do not include the claims made in the paper.
- The abstract and/or introduction should clearly state the claims made, including the contributions made in the paper and important assumptions and limitations. A No or NA answer to this question will not be perceived well by the reviewers.
- The claims made should match theoretical and experimental results, and reflect how much the results can be expected to generalize to other settings.
- It is fine to include aspirational goals as motivation as long as it is clear that these goals are not attained by the paper.

2. Limitations

Question: Does the paper discuss the limitations of the work performed by the authors?

Answer: [\[Yes\]](#)

Justification: We state that our implementation still relies on a fixed overlap schedule and an extra forward pass per player.

Guidelines:

- The answer NA means that the paper has no limitation while the answer No means that the paper has limitations, but those are not discussed in the paper.
- The authors are encouraged to create a separate "Limitations" section in their paper.
- The paper should point out any strong assumptions and how robust the results are to violations of these assumptions (e.g., independence assumptions, noiseless settings, model well-specification, asymptotic approximations only holding locally). The authors should reflect on how these assumptions might be violated in practice and what the implications would be.
- The authors should reflect on the scope of the claims made, e.g., if the approach was only tested on a few datasets or with a few runs. In general, empirical results often depend on implicit assumptions, which should be articulated.
- The authors should reflect on the factors that influence the performance of the approach. For example, a facial recognition algorithm may perform poorly when image resolution is low or images are taken in low lighting. Or a speech-to-text system might not be used reliably to provide closed captions for online lectures because it fails to handle technical jargon.
- The authors should discuss the computational efficiency of the proposed algorithms and how they scale with dataset size.
- If applicable, the authors should discuss possible limitations of their approach to address problems of privacy and fairness.
- While the authors might fear that complete honesty about limitations might be used by reviewers as grounds for rejection, a worse outcome might be that reviewers discover limitations that aren't acknowledged in the paper. The authors should use their best judgment and recognize that individual actions in favor of transparency play an important role in developing norms that preserve the integrity of the community. Reviewers will be specifically instructed to not penalize honesty concerning limitations.

3. Theory assumptions and proofs

Question: For each theoretical result, does the paper provide the full set of assumptions and a complete (and correct) proof?

Answer: [Yes]

Justification: All assumptions required for our theoretical results are explicitly stated. Complete proofs are included in the appendices, with concise proof sketches provided in the main text.

Guidelines:

- The answer NA means that the paper does not include theoretical results.
- All the theorems, formulas, and proofs in the paper should be numbered and cross-referenced.
- All assumptions should be clearly stated or referenced in the statement of any theorems.
- The proofs can either appear in the main paper or the supplemental material, but if they appear in the supplemental material, the authors are encouraged to provide a short proof sketch to provide intuition.
- Inversely, any informal proof provided in the core of the paper should be complemented by formal proofs provided in appendix or supplemental material.
- Theorems and Lemmas that the proof relies upon should be properly referenced.

4. Experimental result reproducibility

Question: Does the paper fully disclose all the information needed to reproduce the main experimental results of the paper to the extent that it affects the main claims and/or conclusions of the paper (regardless of whether the code and data are provided or not)?

Answer: [Yes]

Justification: The paper provides detailed experimental settings.

Guidelines:

- The answer NA means that the paper does not include experiments.
- If the paper includes experiments, a No answer to this question will not be perceived well by the reviewers: Making the paper reproducible is important, regardless of whether the code and data are provided or not.
- If the contribution is a dataset and/or model, the authors should describe the steps taken to make their results reproducible or verifiable.
- Depending on the contribution, reproducibility can be accomplished in various ways. For example, if the contribution is a novel architecture, describing the architecture fully might suffice, or if the contribution is a specific model and empirical evaluation, it may be necessary to either make it possible for others to replicate the model with the same dataset, or provide access to the model. In general, releasing code and data is often one good way to accomplish this, but reproducibility can also be provided via detailed instructions for how to replicate the results, access to a hosted model (e.g., in the case of a large language model), releasing of a model checkpoint, or other means that are appropriate to the research performed.
- While NeurIPS does not require releasing code, the conference does require all submissions to provide some reasonable avenue for reproducibility, which may depend on the nature of the contribution. For example
 - (a) If the contribution is primarily a new algorithm, the paper should make it clear how to reproduce that algorithm.
 - (b) If the contribution is primarily a new model architecture, the paper should describe the architecture clearly and fully.
 - (c) If the contribution is a new model (e.g., a large language model), then there should either be a way to access this model for reproducing the results or a way to reproduce the model (e.g., with an open-source dataset or instructions for how to construct the dataset).
 - (d) We recognize that reproducibility may be tricky in some cases, in which case authors are welcome to describe the particular way they provide for reproducibility. In the case of closed-source models, it may be that access to the model is limited in some way (e.g., to registered users), but it should be possible for other researchers to have some path to reproducing or verifying the results.

5. Open access to data and code

Question: Does the paper provide open access to the data and code, with sufficient instructions to faithfully reproduce the main experimental results, as described in supplemental material?

Answer: [No]

Justification: Due to institutional restrictions and proprietary considerations, the data and code used in this study are not publicly available at this time. However, comprehensive details, including dataset descriptions, model configurations, hyperparameters, and training procedures, are provided in the main text and supplemental materials to facilitate reproducibility.

Guidelines:

- The answer NA means that paper does not include experiments requiring code.
- Please see the NeurIPS code and data submission guidelines (<https://nips.cc/public/guides/CodeSubmissionPolicy>) for more details.
- While we encourage the release of code and data, we understand that this might not be possible, so “No” is an acceptable answer. Papers cannot be rejected simply for not including code, unless this is central to the contribution (e.g., for a new open-source benchmark).
- The instructions should contain the exact command and environment needed to run to reproduce the results. See the NeurIPS code and data submission guidelines (<https://nips.cc/public/guides/CodeSubmissionPolicy>) for more details.
- The authors should provide instructions on data access and preparation, including how to access the raw data, preprocessed data, intermediate data, and generated data, etc.
- The authors should provide scripts to reproduce all experimental results for the new proposed method and baselines. If only a subset of experiments are reproducible, they should state which ones are omitted from the script and why.
- At submission time, to preserve anonymity, the authors should release anonymized versions (if applicable).
- Providing as much information as possible in supplemental material (appended to the paper) is recommended, but including URLs to data and code is permitted.

6. Experimental setting/details

Question: Does the paper specify all the training and test details (e.g., data splits, hyperparameters, how they were chosen, type of optimizer, etc.) necessary to understand the results?

Answer: [Yes]

Justification: The paper explicitly describes datasets, choice of hyperparameters, optimization methods, and computational settings in the experimental sections and appendix.

Guidelines:

- The answer NA means that the paper does not include experiments.
- The experimental setting should be presented in the core of the paper to a level of detail that is necessary to appreciate the results and make sense of them.
- The full details can be provided either with the code, in appendix, or as supplemental material.

7. Experiment statistical significance

Question: Does the paper report error bars suitably and correctly defined or other appropriate information about the statistical significance of the experiments?

Answer: [Yes]

Justification: The paper reports experimental results with clearly defined error bars, calculated as the standard deviation across multiple independent runs.

Guidelines:

- The answer NA means that the paper does not include experiments.

- The authors should answer "Yes" if the results are accompanied by error bars, confidence intervals, or statistical significance tests, at least for the experiments that support the main claims of the paper.
- The factors of variability that the error bars are capturing should be clearly stated (for example, train/test split, initialization, random drawing of some parameter, or overall run with given experimental conditions).
- The method for calculating the error bars should be explained (closed form formula, call to a library function, bootstrap, etc.)
- The assumptions made should be given (e.g., Normally distributed errors).
- It should be clear whether the error bar is the standard deviation or the standard error of the mean.
- It is OK to report 1-sigma error bars, but one should state it. The authors should preferably report a 2-sigma error bar than state that they have a 96% CI, if the hypothesis of Normality of errors is not verified.
- For asymmetric distributions, the authors should be careful not to show in tables or figures symmetric error bars that would yield results that are out of range (e.g. negative error rates).
- If error bars are reported in tables or plots, The authors should explain in the text how they were calculated and reference the corresponding figures or tables in the text.

8. Experiments compute resources

Question: For each experiment, does the paper provide sufficient information on the computer resources (type of compute workers, memory, time of execution) needed to reproduce the experiments?

Answer: **[Yes]**

Justification: The paper clearly specifies the computational resources utilized, including GPU type, memory requirements, execution time per run, and overall compute needed for each experimental setting.

Guidelines:

- The answer NA means that the paper does not include experiments.
- The paper should indicate the type of compute workers CPU or GPU, internal cluster, or cloud provider, including relevant memory and storage.
- The paper should provide the amount of compute required for each of the individual experimental runs as well as estimate the total compute.
- The paper should disclose whether the full research project required more compute than the experiments reported in the paper (e.g., preliminary or failed experiments that didn't make it into the paper).

9. Code of ethics

Question: Does the research conducted in the paper conform, in every respect, with the NeurIPS Code of Ethics <https://neurips.cc/public/EthicsGuidelines>?

Answer: **[Yes]**

Justification: We have thoroughly reviewed the NeurIPS Code of Ethics and confirm that our research fully complies with the guidelines.

Guidelines:

- The answer NA means that the authors have not reviewed the NeurIPS Code of Ethics.
- If the authors answer No, they should explain the special circumstances that require a deviation from the Code of Ethics.
- The authors should make sure to preserve anonymity (e.g., if there is a special consideration due to laws or regulations in their jurisdiction).

10. Broader impacts

Question: Does the paper discuss both potential positive societal impacts and negative societal impacts of the work performed?

Answer: **[NA]**.

Justification: There is no societal impact of the work performed.

Guidelines:

- The answer NA means that there is no societal impact of the work performed.
- If the authors answer NA or No, they should explain why their work has no societal impact or why the paper does not address societal impact.
- Examples of negative societal impacts include potential malicious or unintended uses (e.g., disinformation, generating fake profiles, surveillance), fairness considerations (e.g., deployment of technologies that could make decisions that unfairly impact specific groups), privacy considerations, and security considerations.
- The conference expects that many papers will be foundational research and not tied to particular applications, let alone deployments. However, if there is a direct path to any negative applications, the authors should point it out. For example, it is legitimate to point out that an improvement in the quality of generative models could be used to generate deepfakes for disinformation. On the other hand, it is not needed to point out that a generic algorithm for optimizing neural networks could enable people to train models that generate Deepfakes faster.
- The authors should consider possible harms that could arise when the technology is being used as intended and functioning correctly, harms that could arise when the technology is being used as intended but gives incorrect results, and harms following from (intentional or unintentional) misuse of the technology.
- If there are negative societal impacts, the authors could also discuss possible mitigation strategies (e.g., gated release of models, providing defenses in addition to attacks, mechanisms for monitoring misuse, mechanisms to monitor how a system learns from feedback over time, improving the efficiency and accessibility of ML).

11. Safeguards

Question: Does the paper describe safeguards that have been put in place for responsible release of data or models that have a high risk for misuse (e.g., pretrained language models, image generators, or scraped datasets)?

Answer: [NA].

Justification: The paper poses no such risks.

Guidelines:

- The answer NA means that the paper poses no such risks.
- Released models that have a high risk for misuse or dual-use should be released with necessary safeguards to allow for controlled use of the model, for example by requiring that users adhere to usage guidelines or restrictions to access the model or implementing safety filters.
- Datasets that have been scraped from the Internet could pose safety risks. The authors should describe how they avoided releasing unsafe images.
- We recognize that providing effective safeguards is challenging, and many papers do not require this, but we encourage authors to take this into account and make a best faith effort.

12. Licenses for existing assets

Question: Are the creators or original owners of assets (e.g., code, data, models), used in the paper, properly credited and are the license and terms of use explicitly mentioned and properly respected?

Answer: [Yes]

Justification: All datasets and models used in our experiments are properly credited with citations to their original sources.

Guidelines:

- The answer NA means that the paper does not use existing assets.
- The authors should cite the original paper that produced the code package or dataset.
- The authors should state which version of the asset is used and, if possible, include a URL.

- The name of the license (e.g., CC-BY 4.0) should be included for each asset.
- For scraped data from a particular source (e.g., website), the copyright and terms of service of that source should be provided.
- If assets are released, the license, copyright information, and terms of use in the package should be provided. For popular datasets, paperswithcode.com/datasets has curated licenses for some datasets. Their licensing guide can help determine the license of a dataset.
- For existing datasets that are re-packaged, both the original license and the license of the derived asset (if it has changed) should be provided.
- If this information is not available online, the authors are encouraged to reach out to the asset's creators.

13. New assets

Question: Are new assets introduced in the paper well documented and is the documentation provided alongside the assets?

Answer: [NA].

Justification: The paper does not release new assets.

Guidelines:

- The answer NA means that the paper does not release new assets.
- Researchers should communicate the details of the dataset/code/model as part of their submissions via structured templates. This includes details about training, license, limitations, etc.
- The paper should discuss whether and how consent was obtained from people whose asset is used.
- At submission time, remember to anonymize your assets (if applicable). You can either create an anonymized URL or include an anonymized zip file.

14. Crowdsourcing and research with human subjects

Question: For crowdsourcing experiments and research with human subjects, does the paper include the full text of instructions given to participants and screenshots, if applicable, as well as details about compensation (if any)?

Answer: [NA]

Justification: The paper does not involve crowdsourcing nor research with human subjects.

Guidelines:

- The answer NA means that the paper does not involve crowdsourcing nor research with human subjects.
- Including this information in the supplemental material is fine, but if the main contribution of the paper involves human subjects, then as much detail as possible should be included in the main paper.
- According to the NeurIPS Code of Ethics, workers involved in data collection, curation, or other labor should be paid at least the minimum wage in the country of the data collector.

15. Institutional review board (IRB) approvals or equivalent for research with human subjects

Question: Does the paper describe potential risks incurred by study participants, whether such risks were disclosed to the subjects, and whether Institutional Review Board (IRB) approvals (or an equivalent approval/review based on the requirements of your country or institution) were obtained?

Answer: [NA]

Justification: The paper does not involve crowdsourcing nor research with human subjects.

Guidelines:

- The answer NA means that the paper does not involve crowdsourcing nor research with human subjects.

- Depending on the country in which research is conducted, IRB approval (or equivalent) may be required for any human subjects research. If you obtained IRB approval, you should clearly state this in the paper.
- We recognize that the procedures for this may vary significantly between institutions and locations, and we expect authors to adhere to the NeurIPS Code of Ethics and the guidelines for their institution.
- For initial submissions, do not include any information that would break anonymity (if applicable), such as the institution conducting the review.

16. Declaration of LLM usage

Question: Does the paper describe the usage of LLMs if it is an important, original, or non-standard component of the core methods in this research? Note that if the LLM is used only for writing, editing, or formatting purposes and does not impact the core methodology, scientific rigorousness, or originality of the research, declaration is not required.

Answer: [NA]

Justification: In this work, LLMs were employed solely for improving language clarity.

Guidelines:

- The answer NA means that the core method development in this research does not involve LLMs as any important, original, or non-standard components.
- Please refer to our LLM policy (<https://neurips.cc/Conferences/2025/LLM>) for what should or should not be described.

A Proofs of Theoretical Results

A.1 Proof of 4.1

Proof. Let $\mathcal{F} = \{f_\phi(x, y^+, z) = \mathcal{L}_m(x, y^+, z; \phi) : \phi \in \Phi\}$. For brevity write $\mu(f) = \mathbb{E}[f]$ and $\hat{\mu}_n(f) = \frac{1}{n} \sum_{i=1}^n f(X_i)$ with $X_i = (x_i, y_i^+, z_i)$; here $z_i \sim \sigma_\eta$ is drawn *dependent* on the anchor (x_i, y_i^+) . We first decouple this dependence.

Step 1. Decoupling via ghost samples. Introduce i.i.d. *ghost* negatives $\tilde{z}_i \sim \sigma_\eta(x_i)$ and define $\tilde{X}_i = (x_i, y_i^+, \tilde{z}_i)$. Because z_i, \tilde{z}_i are conditionally independent given the anchor, Bennet's coupling gives

$$\Pr(|\hat{\mu}_n(f) - \mu(f)| > t) \leq 2 \Pr\left(\left|\frac{1}{n} \sum_{i=1}^n (f(X_i) - f(\tilde{X}_i))\right| > \frac{t}{2}\right). \quad (17)$$

It therefore suffices to bound the righthand deviation, which now has *independent* summands.

Step 2. Variance proxy with ambiguous density. For each $f \in \mathcal{F}$ write $\xi_i = f(X_i) - f(\tilde{X}_i)$. Conditioned on (x_i, y_i^+) and under 4.1&4.2,

$$|\xi_i| \leq L |s(x_i, z_i) - s(x_i, \tilde{z}_i)| \leq 2L(m - \varepsilon), \quad (18)$$

while $\text{Var}(\xi_i) \leq \mathbb{E}[\xi_i^2] \leq 4L^2\rho(m - \varepsilon)^2$. Define $\sigma^2 = 4L^2\rho(m - \varepsilon)^2$ and $M = 2L(m - \varepsilon)$.

Step 3. Localised Rademacher complexity. Let $S_f^2 = \frac{1}{n} \sum_{i=1}^n (\xi_i - \mathbb{E}[\xi_i])^2$ be the empirical variance of f . Bartlett and Mendelson's local Rademacher complexity [Bartlett et al., 2005] yields with probability $\geq 1 - \delta/2$

$$\sup_{f \in \mathcal{F}} |\hat{\mu}_n(f) - \mu(f)| \leq \underbrace{\frac{4}{n} \mathfrak{R}_n(\mathcal{F})}_{\text{estimation}} + \underbrace{6M \sqrt{\frac{\log(4/\delta)}{2n}}}_{\text{concentration}}, \quad (19)$$

where the (global) Rademacher complexity is $\mathfrak{R}_n(\mathcal{F}) = \mathbb{E}[\sup_{f \in \mathcal{F}} \frac{1}{n} \sum_{i=1}^n \varepsilon_i f(X_i)]$.

Step 4. DudleyLedouxTalagrand chaining. Equip \mathcal{F} with pseudometric $d(f, f')^2 = \mathbb{E}[(f - f')^2]$. Because f_ϕ is *LLipschitz* in ϕ under d , its covering number satisfies $\log \mathcal{N}(\mathcal{F}, d, \eta) \leq d_{\text{eff}} \log(4L/\eta)$. Applying Dudley's integral and LedouxTalagrand contraction,

$$\begin{aligned} \mathfrak{R}_n(\mathcal{F}) &\leq \frac{12L(m - \varepsilon)}{\sqrt{n}} \int_0^M \sqrt{\frac{\log \mathcal{N}(\mathcal{F}, d, \eta)}{n}} d\eta \\ &\leq \frac{12L(m - \varepsilon)}{\sqrt{n}} \int_0^M \sqrt{\frac{d_{\text{eff}} \log \frac{4L}{\eta}}{n}} d\eta = \frac{6L(m - \varepsilon)}{\sqrt{n}} \sqrt{\frac{\pi d_{\text{eff}}}{2}} (1 + o(1)). \end{aligned} \quad (20)$$

Substituting (20) into (19) and combining with (17), with probability $\geq 1 - \delta$

$$\sup_{\phi \in \Phi} |\mathcal{R}(\phi) - \mathcal{R}_n^B(\phi)| \leq \frac{24L(m - \varepsilon)}{(1 - \rho)\sqrt{n}} \sqrt{d_{\text{eff}} \log \frac{4e}{m - \varepsilon}} + \frac{32L^2}{(1 - \rho)n} + \frac{8L(m - \varepsilon)}{1 - \rho} \sqrt{\frac{\log \frac{4}{\delta}}{n}}. \quad (21)$$

Optimising constants (absorbing the last squareroot term into the first) yields (14). \square

A.2 Proof of Theorem 4.2

Proof. We derive (15) via five steps.

Step 1. A Kary packing of ambiguous negatives. Fix $K = \lfloor \frac{\rho n}{4} \rfloor \geq 2$. For each $\theta \in \{0, 1\}^K$ construct \mathbb{P}_θ as follows. Anchors (x, y^+) are drawn identically across θ . Conditionally, partition the anchor set into K groups G_1, \dots, G_K of equal size $|G_k| = \lfloor n/K \rfloor$. For $i \in G_k$,

$$z_i \sim \begin{cases} q_0(\cdot | x_i) & \text{if } \theta_k = 0, \\ q_1(\cdot | x_i) & \text{if } \theta_k = 1, \end{cases} \quad (22)$$

where q_0 selects *benign* negatives ($s(x_i, z) = s(x_i, y_i^+) + m$), and q_1 selects *ambiguous* negatives ($s(x_i, z) = s(x_i, y_i^+) + \varepsilon$). This yields $M = 2^K$ candidate distributions; Hamming distance $H(\theta, \theta')$ controls their difficulty.

Step 2. KL pairwise bound. Let $\ell(\theta, \theta') = \text{KL}(\mathbb{P}_\theta^n \| \mathbb{P}_{\theta'}^n)$. Because different groups are independent,

$$\begin{aligned} \ell(\theta, \theta') &= \sum_{k=1}^K H(\theta_k, \theta'_k) |G_k| \text{KL}(q_0 \| q_1) \\ &\stackrel{(*)}{\leq} H(\theta, \theta') \left\lceil \frac{n}{K} \right\rceil \frac{(\varepsilon)^2}{2(m-\varepsilon)^2} \leq \frac{\rho \varepsilon^2 n}{(m-\varepsilon)^2}, \end{aligned} \quad (23)$$

where $(*)$ uses Pinsker's linearisation and the fact that changing the similarity by $\pm \varepsilon$ alters the triplet density by at most $\varepsilon/(m-\varepsilon)$ under Lipschitzness.

Step 3. Assouadtype reduction (general M). Define $\Delta(\hat{\phi}, \theta) = \mathcal{R}(\hat{\phi}) - \mathcal{R}(\phi^*)$ under \mathbb{P}_θ . By margin monotonicity, for any k $\mathbb{E}_{\mathbb{P}_\theta}[\Delta(\hat{\phi}, \theta)] \geq (m-2\varepsilon) \Pr_{\mathbb{P}_\theta}(\hat{\theta}_k \neq \theta_k)$, where $\hat{\theta}_k$ is the majority vote among group G_k (*plugin decoder*). Averaging over θ and summing k ,

$$\frac{1}{M} \sum_{\theta} \mathbb{E}_{\mathbb{P}_\theta}[\Delta(\hat{\phi}, \theta)] \geq \frac{(m-2\varepsilon)}{K} \sum_{k=1}^K (1 - \bar{\alpha}_k), \quad \bar{\alpha}_k = \frac{1}{M} \sum_{\theta} \Pr_{\mathbb{P}_\theta}(\hat{\theta}_k = \theta_k). \quad (24)$$

Step 4. BretagnolleHuber bound (multiway). For any k consider the binary experiment $\theta_k = 0$ versus 1, mixing uniformly over other coordinates. Using BretagnolleHuber's inequality and (23),

$$\bar{\alpha}_k \leq \frac{1}{2} \sqrt{\text{KL}_{\text{mix}}} \leq \frac{1}{2} \sqrt{\frac{2\rho\varepsilon^2 n}{(m-\varepsilon)^2}} \stackrel{(\dagger)}{\leq} 1 - \frac{\rho}{8} \sqrt{\frac{\log \frac{1}{4\delta}}{n}}, \quad (25)$$

provided (\dagger) enforces $n \geq \frac{32\rho\varepsilon^2}{(m-\varepsilon)^2} \log \frac{1}{4\delta}$, which is milder than our final requirement.

Step 5. Final lower bound. Substituting (25) into (24) and recalling $K = \lfloor \rho n/4 \rfloor$,

$$\begin{aligned} \sup_{\Psi} \inf_{\mathbb{P} \in \{\mathbb{P}_\theta\}} \mathbb{E}_{\mathbb{P}}[\Delta(\Psi, \mathbb{P})] &\geq (m-2\varepsilon) \left(\frac{\rho}{8} \sqrt{\frac{\log \frac{1}{4\delta}}{n}} \right) \\ &\quad + \underbrace{(m-2\varepsilon) \left(\frac{1}{n} \sum_{k=1}^K \frac{1}{|G_k|} \right) \cdot \frac{L(m-2\varepsilon)}{8}}_{= \frac{\rho^2(m-2\varepsilon)}{16n}} \\ &\geq \frac{\rho(m-2\varepsilon)}{32} \sqrt{\frac{\log \frac{1}{4\delta}}{n}} + \frac{\rho^2 L(m-2\varepsilon)^2}{128n}, \end{aligned} \quad (26)$$

which is the desired (15). \square

A.3 Proof of Proposition 4.1

Proof. The argument proceeds in four steps: (I) gradient lower bound, (II) onestep recurrence with stochastic correction, (III) nonlinear discrete Grönwall inequality, and (IV) closedform evaluation for the logistic schedule.

Step I: Gradient lower bound. Let (x, y^+) be the anchorpositive pair in a minibatch and z^- the hardest negative selected by the sampler. Denote $\delta_\eta = s_\eta(x, z^-) - s_\eta(x, y^+) \leq -\Delta_\eta$. By definition of CLA, the *signed* gradient of the triplet loss $\ell_\eta = [m + \delta_\eta]_+$ w.r.t. $s_\eta(x, z^-)$ equals $g_\eta = 1 + \beta \Delta_\eta \geq 1 + \beta \Delta_{\eta-1}$. Using Lipschitzness (Assumption 4.2) and the update $s_{\eta+1}(x, z^-) = s_\eta(x, z^-) - \eta_{\text{lr}} g_\eta / B$ while $s_\eta(x, y^+)$ increases by at most η_{lr} / B , we obtain

$$\Delta_{\eta+1} \leq \Delta_\eta - \eta_{\text{lr}} \left(1 + \beta \Delta_\eta\right) \frac{m - \varepsilon}{LB} + \frac{\eta_{\text{lr}} \xi_\eta}{B}, \quad |\xi_\eta| \leq \varepsilon, \quad (27)$$

where the martingale term ξ_η captures sampling noise.

Step II: Highprobability martingale control. Define the filtration \mathcal{F}_η generated by the stochastic gradient history and let $M_\eta = \sum_{t=0}^{\eta-1} \xi_t$. AzumaHoeffding implies $\Pr(|M_\eta| > \varepsilon \sqrt{2\eta \log(1/\delta)}) \leq \delta$. Conditioning on the complementary event \mathcal{E}_δ , we replace ξ_η in (27) by its upper bound $\varepsilon \sqrt{2 \log(1/\delta) / \eta}$ and proceed deterministically.

Step III: Nonlinear discrete Grönwall. Set $u_\eta = \Delta_\eta / (m - \varepsilon)$, $\lambda = \eta_{\text{lr}} / (LB)$. Inequality (27) on \mathcal{E}_δ becomes $u_{\eta+1} \leq u_\eta - \lambda(1 + \beta(m - \varepsilon)u_\eta) + \lambda\varepsilon'$ with $\varepsilon' = \varepsilon^2 \sqrt{2 \log(1/\delta) / ((m - \varepsilon)LB)}$. Ignoring ε' (absorbed into initial condition) and dividing by $1 + \beta(m - \varepsilon)u_\eta$,

$$\frac{u_{\eta+1}}{1 + \beta(m - \varepsilon)u_{\eta+1}} \leq \frac{u_\eta}{1 + \beta(m - \varepsilon)u_\eta} (1 - \lambda\beta(m - \varepsilon)) \stackrel{\text{def}}{=} \hat{q} v_\eta, \quad v_\eta = \frac{u_\eta}{1 + \beta(m - \varepsilon)u_\eta}.$$

Iterating yields $v_\eta \leq \hat{q}^\eta v_0$. Because $u \mapsto v = u / (1 + \beta(m - \varepsilon)u)$ is invertible, $u_\eta \leq \frac{v_0 \hat{q}^\eta}{1 - \beta(m - \varepsilon)v_0 \hat{q}^\eta} \leq v_0 \hat{q}^\eta \exp(\beta(m - \varepsilon)v_0 \hat{q}^\eta)$, where we used $1/(1 - x) \leq e^x$.

Step IV: Closedform for logistic $\alpha(\eta)$. With $\alpha(\eta) = \alpha_{\text{early}} + (\alpha_{\text{late}} - \alpha_{\text{early}})(1 + e^{-\gamma(\eta - \eta_0)})^{-1}$, we bound $\bar{\alpha}_\eta \geq \alpha_{\text{late}} + (\alpha_{\text{early}} - \alpha_{\text{late}}) \frac{\log(1 + e^{\gamma(\eta - \eta_0)})}{\gamma\eta}$, whence $\exp(\bar{\alpha}_\eta) \geq c_0 e^{-c_1/\eta} e^{\alpha_{\text{late}}}$, for constants $c_0, c_1 > 0$. Collecting factors and restoring $\Delta_\eta = u_\eta(m - \varepsilon)$ gives

$$\Delta_\eta \leq \Delta_0 \exp(-\kappa(e^{\bar{\alpha}_\eta} - 1)) \leq \Delta_0 \exp(-\frac{1}{2}\kappa c_0 e^{\alpha_{\text{late}}}\eta + \frac{\kappa c_1}{2}).$$

Setting $\alpha_{\text{late}} \leq -c_\alpha$ transforms the linear-in- η exponent into $-\Theta(\eta^2)$, producing the superexponential rate (16). \square

B Algorithm

Algorithm 1 summarizes the computational flow of our BACL.

C Dataset Details

LAION-400M [Schuhmann et al., 2021]

A web-scale imagetext corpus containing **400 M** imagecaption pairs filtered with a CLIP similarity threshold. We keep the official training partition (398 M pairs) for unsupervised pre-training and randomly sample 50 k pairs for validation. Retrieval evaluation follows the standard 30 k imagequery split, reporting R@1/5/10 and mAP.

WebVid-10M [Bain et al., 2021]

Consists of **10.7 M** 5-second video clips scraped from stock-footage websites, each accompanied by a noisy user caption. We adopt the pre-train split (10.1 M) for curriculum mining and the canonical val split (40 k) for retrieval, reporting R@K ($K=1, 5, 10$) and nDCG.

VAST-27M [Chen et al., 2023]

A tri-modal dataset (*video, audio, subtitle*) with **27 M** clip-level samples drawn from instructional and documentary sources. We use the official train/val/test splits (26 M / 0.5 M / 0.5 M) and follow Chen et al. [2023] to evaluate clip-level classification with Accuracy, macro-F1, and Recall.

Algorithm 1 BACL: Boundary-aware Curriculum Learning for Multimodal Alignment

Require: Paired corpus $\mathcal{D} = \{(x_i, y_i)\}_{i=1}^N$, similarity margin ε , epochs E , batch size B , curriculum parameters $(\alpha_{\text{early}}, \alpha_{\text{late}}, \gamma, \eta_0)$, Gumbel temperature τ , local-loss weight λ_{local}

Ensure: Trained encoders $\phi_{\mathcal{X}}, \phi_{\mathcal{Y}}$

- 1: **(Init)** Pre-train $\phi_{\mathcal{X}}, \phi_{\mathcal{Y}}$ on \mathcal{D} with the global contrastive loss to obtain θ^0
- 2: Build modality indices using embeddings $\mathbf{z}(x) = \phi_{\mathcal{X}}(x)$ and $\mathbf{z}(y) = \phi_{\mathcal{Y}}(y)$
- 3: **for** $\eta = 1$ **to** E **do**
- 4: **for** each mini-batch $\mathcal{B} \subset \mathcal{D}$ of size B **do**
- 5: Encode positives: $\mathbf{z}_x \leftarrow \phi_{\mathcal{X}}(x)$, $\mathbf{z}_y \leftarrow \phi_{\mathcal{Y}}(y)$ for $(x, y) \in \mathcal{B}$
- 6: Retrieve candidate negatives $\{\mathbf{z}_n\}$ s.t. $|s(\mathbf{z}_x, \mathbf{z}_n) - s(\mathbf{z}_x, \mathbf{z}_y)| \leq \varepsilon$
- 7: Compute boundary scores $\text{BS}(\mathbf{z}_x, \mathbf{z}_n) = s(\mathbf{z}_x, \mathbf{z}_n) - s(\mathbf{z}_x, \mathbf{z}_y)$
- 8: Policy network π_{θ} produces raw scores $\{u_n\}$
- 9: **Curriculum scheduling:**
 $\alpha(\eta) = \alpha_{\text{early}} + (\alpha_{\text{late}} - \alpha_{\text{early}})(1 + e^{-\gamma(\eta - \eta_0)})^{-1}$
 $d(\mathbf{z}_n) = \max\{0, \text{BS}(\mathbf{z}_x, \mathbf{z}_n)\}$
 $\hat{u}_n = u_n - \alpha(\eta) d(\mathbf{z}_n)$
- 10: Sample k negatives via Gumbel-Softmax: $\tilde{p}_n \propto \exp((\hat{u}_n + g_n)/\tau)$
- 11: Assemble hardest negative $z^- = \arg \max_n \tilde{p}_n$
- 12: **Global loss** $\mathcal{L}_{\text{contrast}}$ for positives vs. sampled negatives
- 13: **Local attention:** compute $\mathbf{A}^{(+)}$ for (x, y) , $\mathbf{A}^{(-)}$ for (x, z^-) ,
 $\Delta \mathbf{A} = |\mathbf{A}^{(+)} - \mathbf{A}^{(-)}|$,
 $\mathbf{A}^b = \mathbf{A}^{(-)} \cdot (1 + \beta \Delta \mathbf{A})$,
 $\mathcal{L}_{\text{local}} = \sum_{(i,j) \in \Omega} -\log(\mathbf{A}^b(i, j))$
- 14: **Total loss:** $\mathcal{L}_{\text{main}} = \mathcal{L}_{\text{contrast}} + \lambda_{\text{local}} \mathcal{L}_{\text{local}}$
- 15: Update $\phi_{\mathcal{X}}, \phi_{\mathcal{Y}}, \pi_{\theta}$ via back-prop on $\mathcal{L}_{\text{main}}$
- 16: **end for**
- 17: **end for**
- 18: **return** $\phi_{\mathcal{X}}, \phi_{\mathcal{Y}}$

WavText5K [Deshmukh et al., 2022]

An audiotext retrieval benchmark of **5 123** audio clips paired with crowdsourced captions. We use the public train/val/test splits (3 742 / 640 / 741) and report R@1/5/10 and Mean Reciprocal Rank.

All datasets are released under permissive licenses (e.g. CC-BY-4.0); we strictly follow the original creators data-usage terms.

D Baseline Details

Table 3 summarises the key design choices of all competing methods.

Exclusion criteria. Baselines that require proprietary data (e.g. Flamingo) or are not publicly released were excluded for fairness and reproducibility.

E Implementation Details

Encoders. Unless otherwise stated, we freeze CLIP ViT-B/16 (visual), GELU-RoBERTa (text), and CLAP PANN14 (audio) backbones, inserting a 4-layer cross-modal Transformer with hidden size 512 as the trainable fusion module. For tri-modal experiments we add a separate audio adapter and share the projection head across modalities.

Boundary-aware Negative Sampler (BNS). The policy network π_{θ} is a two-layer MLP (512-128-1) with SiLU activation. Gumbel-Softmax temperature τ is initialised at 0.7 and linearly annealed to 0.1. Logistic schedule parameters are set to $\alpha_{\text{early}}=0.3$, $\alpha_{\text{late}}= -0.5$, $\gamma=1.5$, and η_0 equal to 40% of the total pre-training epochs.

Table 3: Summary of baseline methods used for comparison.

Method	Neg. Strategy	Local loss	Modalities
CLIP [Radford et al., 2021]	Uniform	–	I+T
ALIGN [Jia et al., 2021]	Uniform	–	I+T
VSE++ [Faghri et al., 2018]	Batch max	–	I+T
UNITER [Chen et al., 2020]	Batch hard	Region	I+T
ALBEF [Li et al., 2021]	Batch hard	Cross-attn	I+T
ViLT [Kim et al., 2021]	Uniform	Token	I+T
BLIP [Li et al., 2022]	Momentum hard	Gen. aux	I+T
BLIP-2 [Li et al., 2023]	Frozen CLIP	Gen. aux	I+T+L
DCOT [Wang et al., 2023]	OT curriculum	–	I+T
Emergence [Tjandrasuwita et al., 2025]	–	Analysis	V/A/T
CoMM [Dufumier et al., 2024]	InfoNCE split	–	V/A/T
M3-JEPA [Lei et al., 2024]	Alternating	–	V/A/T
GRAM [Cicchetti et al., 2024]	Volume contrast	–	V/A/T/D
CLAP [Elizalde et al., 2022]	Uniform	–	A+T
MIL-NCE [Miech et al., 2020a]	MIL hard	–	V+T

Table 4: Overall accuracy (%) on **VQA^{v2} test-std**.

Method	Neg. Strategy	Accuracy
ViLT [Kim et al., 2021]	Uniform	71.2
ALBEF [Li et al., 2021]	Batch max violation	74.4
BLIP [Li et al., 2022]	Momentum + Hard Neg.	77.3
BLIP2 [Li et al., 2023]	Frozen Image + LLM	80.0
M3JEPA [Lei et al., 2024]	Alternating	79.1
CLIP+BACL (Ours)	Curriculum	73.8
BLIP+BACL (Ours)	Curriculum	79.2
M3JEPA+BACL (Ours)	Curriculum	82.3

Contrastive Local Attention (CLA). We apply CLA to the last cross-attention layer, selecting the top 15% token pairs ranked by ΔA (Eq. (10)) as Ω . The gain coefficient β is fixed at 2.0 and λ_{local} at 0.3.

Training. All models are pre-trained for ten epochs on each dataset with a global batch size of 16 384 (512 per GPU, 32 \times A100). AdamW weight decay is set to 1e-2 and learning rate to 2e-4 with cosine decay. Finetuning hyper-parameters for VQA v2 and NLVR2 are listed in Appendix F. Each full run on LAION-400M takes approximately 36 h on the aforementioned cluster.

Evaluation. Retrieval metrics are computed with FAISS IVF4096, PQ32 indexing; classification uses the official task scripts. All reported numbers are averaged over three seeds.

F Extended Experiments

F.1 Fine-grained multimodal reasoning

To assess whether the boundary-aware curriculum (BACL) also enhances finegrained multimodal reasoning, we finetune the BACL-pretrained encoders on two widely used benchmarks: Visual Question Answering (VQA v2) and Natural Language for Visual Reasoning (NLVR2). We compare against strong visionlanguage models that either employ uniform negatives or a singleshot hardnegative strategy during pretraining.

VQA v2. We finetune for five epochs on the 443 k QA pairs of the VQA v2 training split with a batch size of 256, AdamW ($\beta_1 = 0.9$, $\beta_2 = 0.98$) and a peak learning rate of 2×10^{-5} . We report the test-std overall accuracy from the official evaluation server.

Table 5: Accuracy (%) on **NLVR2** test-P.

Method	Neg. Strategy	Accuracy
ViLT [Kim et al., 2021]	Uniform	79.9
ALBEF [Li et al., 2021]	Batchmaxviolation	82.5
BLIP [Li et al., 2022]	Momentum + HardNeg.	86.7
BLIP2 [Li et al., 2023]	Frozen Image + LLM	90.3
M3JEPA [Lei et al., 2024]	Alternating	89.0
CLIP+BACL (Ours)	Curriculum	84.2
BLIP+BACL (Ours)	Curriculum	87.9
M3JEPA+BACL (Ours)	Curriculum	90.8

NLVR2. We adopt the 2+1 finetuning schedule of Li et al. [2022] on the 86k NLVR2 training examples, training for three epochs with a peak learning rate of 1×10^{-5} and reporting accuracy on the public test-P set.

Discussion. Across both datasets, incorporating the boundaryaware curriculum consistently improves accuracy over the corresponding backbones. Notably, *M3JEPA+BACL* achieves stateofheart results on NLVR2 (90.8%) and pushes VQA v2 accuracy to 82.3%, confirming that progressively focusing on ambiguous negatives does not harm, and in fact reinforces, finegrained visual reasoning capabilities while preserving the global retrieval gains reported in Tables 1a2b.

F.2 Interpretability of CLA via Alignment-Error Localisation

To quantify whether CLA pinpoints fine-grained mismatches, we compute *Alignment-Error Localisation* (AEL): the percentage of human-tagged mismatch tokens covered by the top-10% cells of the cross-modal discrepancy map ΔA . As shown in Table 6, BACL improves localisation by ~ 11 pp on average.

For each anchor (x, y^+) we obtain a positive cross-modal attention map $A^{(+)}$ and, using the BNS-selected hardest negative y^- , a negative map $A^{(-)}$. We form a discrepancy map

$$\Delta A = |A^{(+)} - A^{(-)}| \quad (\text{element-wise absolute difference}). \quad (28)$$

We minmax normalise ΔA per instance and select the top-10% cells by value as the *salient discrepancy set*. For models without an explicit cross-attention module (pure dual encoders), we compute token saliencies via similarity gradients and construct an outer-product proxy, ΔA is then defined analogously on these proxy maps.

We curate two evaluation subsets with ambiguous negatives: *LAION-400M AmbNeg-1k* (imagetext) and *WebVid-HardNeg 800* (videotext). Three trained annotators per example mark *mismatch spans*: image patches/frames and caption tokens that explain why y^- is incorrect despite high global similarity (guidelines cover object identity, attributes, relations, and temporal consistency). We resolve disagreements by majority vote; agreement was substantial (Fleiss κ in the substantial range). AEL is computed as the fraction of annotated tokens covered by the top-10% ΔA cells and averaged across examples.

Global retrieval scores do not reveal *where* a model finds evidence to reject near-miss negatives. AEL instead measures whether the models *local* discrepancy signal aligns with human-identified error spans exactly the behaviour CLA is designed to induce. Table 6 shows consistent gains of ~ 11 pp AEL for BACL over a strong CLIP baseline across both imagetext and videotext settings. The improvement persists when we vary the saliency budget from 515% (ranking unchanged) and remains significant under paired bootstrapping over examples. On WebVid, we aggregate frame-level maps with max-pooling over time; using mean-pooling yields similar trends. CLA does not merely boost global retrieval; it systematically aligns the models token-level discrepancy signal with human-marked error spans, yielding the ~ 11 pp AEL improvement in Table 6.

Table 6: **AEL (%) \uparrow** . Higher is better.

Dataset	vanilla CLIP	BACL (ours)	Δ (pp)
LAION-400M AmbNeg-1k	46.2	57.8	+11.6
WebVid-HardNeg 800	39.6	50.5	+10.9
Average	42.9	54.2	+11.3

F.3 Sensitivity to Data Scale

We train CLIP \pm BACL on three LAION subsets with identical hyper-parameters (5 epochs; ViT-B/32). Table 7 shows that the relative gain remains $\approx 30\%$ from 10^8 to 10^9 pairs.

Table 7: **Scaling on LAION**. R@1 on zero-shot imagetext retrieval.

Subset	# pairs	CLIP R@1	CLIP+BACL R@1	Rel. gain
100M	1.0×10^8	31.5	40.8	+29.5%
400M	4.0×10^8	35.2	46.5	+32.1%
1B *	1.0×10^9	38.9	50.4	+29.6%

* One-billion subset constructed by uniform sampling from LAION-5B with standard filtering.

F.4 Runtime, Throughput, and Memory Footprint

We jointly benchmark throughput, iteration rate, and peak memory / max batch under a consistent setup. Table 8 consolidates all measurements and indicates a modest overhead overall (< 8% time, ~ 1.7 GB memory).

Table 8: **Consolidated efficiency metrics** on LAION-400M (batch=512). Iteration rate measured on $8 \times$ A100-40GB; memory on a single A100-40GB.

Setting	Images/s	Δ (%)	Iters/s	Δ (%)	Peak (GB)	Δ (GB)	Max batch
CLIP baseline	330		8.2k		29.6		512
+ BNS			7.9k	-3.6	30.0	+0.4	512
+ CLA	304	-7.9			31.1	+1.5	480
BACL (BNS+CLA)					31.3	+1.7	480

“” = not measured under the given setup.